

Y3, N21/5 : 6/1903

TECHNICAL NOTE 1903

By Paul W. Huber, Cliff E. Fitton, Jr., and F. Delpino

Langley Aeronautical Laboratory
Langley Air Force Base, Va.



Washington

July 1949

BUSINESS, SCIENCE
& TECHNOLOGY DEPT.

JUL 28 1949

NATIONAL ADVISORY COMMITTEE FOR AERONAUTICS

TECHNICAL NOTE 1903

EXPERIMENTAL INVESTIGATION OF MOVING PRESSURE DISTURBANCES AND SHOCK WAVES AND CORRELATION WITH ONE-DIMENSIONAL UNSTEADY-FLOW THEORY

By Paul W. Huber, Cliff E. Fitton, Jr., and F. Delpino

SUMMARY

Experimental pressure-time measurements, along with schlieren photographs of the unsteady-flow phenomena initiated in constant-cross-sectional-area passages, are presented. The methods of calculation of the flow phenomena are based on the assumptions of one-dimensional, nonviscous, unsteady flow. The unsteady flow - which is studied both experimentally and theoretically - includes propagation of pressure disturbances, which may be either expansion zones or discontinuous compression fronts, temperature contact discontinuities in the flow, and the reflections and interactions of these flow quantities. A very close agreement is shown between the experimental measurements of the flow and the flow predicted by the theory over a wide range of flow conditions. Special instrumentation was developed during these tests which greatly facilitated the measurement of the unsteady-flow phenomena.

INTRODUCTION

The important role played by moving pressure disturbances in various aerodynamic configurations is becoming increasingly apparent. In pulse-jet engines and heat engines, such as the comprex or pressure exchanger (reference 1), moving compression and expansion waves are alternately used to compress the gas before heat is added and to expand the hot gases in the same passage, in much the same manner as is obtained by the action of a mechanical piston. The action of pressure disturbances in the subsonic part of a supersonic diffuser is recognized as causing an instability of the shock wave with a resulting adverse effect on pressure-recovery efficiency. In some cases (reference 2), constant-geometry supersonic diffusers have been started at Mach numbers below the theoretical starting Mach number (based on steady-flow considerations) by means of pressure disturbances. In steady-flow-type burners, as well as in combustion engines, the action of pressure disturbances and detonation waves produce a marked change in the combustion phenomena.

Although these actions of pressure disturbances in aerodynamic and thermodynamic phenomena have become recognized and their effects have been partly evaluated from the general trend of experimental tests, the amount of available experimental data has been insufficient to verify the theory of unsteady flow. This lack of fundamental experimental data has been partly due to a lack of instrumentation capable of responding with any degree of accuracy to the rapidly changing conditions of this type of flow.

In general, many of the one-dimensional unsteady-flow cases of fundamental interest can be treated mathematically with existing methods. (See references 3 to 6.) These methods, in their present form, however, are not applicable to viscous flows, flows involving heat transmission, or flows of more than one dimension, which are usually the flows of engineering interest.

The purpose of the present investigation is to compare the results of an experimental study of one-dimensional unsteady flow with results based on the theory of one-dimensional, nonviscous, unsteady flow. A better knowledge of the gas dynamics of this simple type of unsteady flow should prove to be of great assistance in the study of the more complicated flows. As a secondary objective, correlation of theory and experiment has been used to determine the value of instrumentation for measurements of one-dimensional, nonviscous, unsteady flow.

SYMBOLS

p	pressure, atmospheres
u	flow velocity, feet per second
a	velocity of sound, feet per second
t	time, seconds
T	temperature, degrees Fahrenheit
γ	ratio of specific heats at constant pressure to specific heats at constant volume
x	distance, inches
M	Mach number in stationary shock coordinates $\left(\frac{V}{a}\right)$
V	flow velocity in stationary shock coordinates, feet per second
W	velocity of propagation of shock, feet per second

E voltage, volts
l length, inches
 Δp pressure change at crystal due to given pressure front

Subscripts:

a standard atmospheric (29.92 in. Hg)
O high-pressure chamber before diaphragm burst
l low-pressure chamber before diaphragm burst
b before reflection
c after reflection
22 between temperature contact discontinuity and expansion,
before reflection
2 between temperature contact discontinuity and shock, before
reflection
3 between reflected shock and end of low-pressure chamber
4 between reflected expansion and end of high-pressure chamber
L low-pressure chamber
H high-pressure chamber

Superscripts:

' high-pressure side of shock
" low-pressure side of shock

THEORETICAL METHOD

The fundamental relationships for the propagation of plane disturbances of finite amplitude were first derived by Riemann in 1859 for one-dimensional isentropic flow. (See references 3 and 7.) The derivation showed that the propagation of a large disturbance can be treated as the propagation of an infinite number of small disturbances where each small disturbance is propagated at a velocity with respect to the fluid equal to the velocity of sound at that point. If the fluid at that point has a flow velocity of u , then the velocity of propagation of this point on the disturbance is $a \pm u$, where a is

the velocity of sound and the plus sign or minus sign is used if the point is being propagated in the direction of flow or against the direction of flow, respectively. For a streamline of constant cross-sectional area and for a fluid which has a constant value of γ , a disturbance propagated in the direction of flow was shown to produce no change in the quantity of the flow $u - \frac{2}{\gamma - 1} a$ through which it has been propagated; whereas a disturbance propagated against the direction of flow was shown to produce no change in the quantity $u + \frac{2}{\gamma - 1} a$. The propagation of expansion fronts on these disturbances was shown to be such as to make the expansion fronts less steep with time (that is, spreading expansion zones); whereas compression fronts were shown to become more steep with time and eventually to become discontinuous pressure fronts (shocks). From this result, it can be concluded that the shape (the shape being the pressure distribution along the axis of propagation) of any finite isentropic disturbance continually changes with time. In order to calculate the shape of a disturbance at any given point in time, therefore, the shape must obviously be known at some earlier time. If an experimental measurement on the moving disturbance is not trusted, then the time and conditions under which the disturbance was generated must be known (time = 0).

Classical methods for the treatment of disturbances from initial conditions which are known include the following:

1. Assumption that a piston rapidly accelerates to a given velocity which is then held constant. This acceleration of the piston generates a compression front which moves ahead of the piston, while the fluid behind the front flows at the velocity of the piston. Deceleration of the piston to rest consequently generates an expansion zone which moves ahead of the piston and reduces the fluid velocity to zero.

2. Assumption that a diaphragm which separates a chamber of high pressure from a chamber of low pressure is suddenly burst. In this treatment, a compression front is propagated into the low-pressure chamber; whereas an expansion zone is propagated into the high-pressure chamber. The movement of the compression front is such as to compress the fluid in the low-pressure chamber to an intermediate pressure and to accelerate the compressed fluid in the direction of the front. The movement of the expansion zone is such as to reduce the pressure in the high-pressure chamber to the same intermediate pressure and to accelerate the expanded fluid in a direction opposite to the front. A temperature contact discontinuity appears behind the compression and moves in the direction of fluid flow. This surface of discontinuity is the boundary between gas particles expanded from the high-pressure chamber and particles compressed from the low-pressure chamber.

The diaphragm method was chosen because it seemed somewhat easier to reproduce experimentally.

In 1932, Schardin (reference 8) performed calculations from which the pressure distribution along tubes of constant cross section can be found at certain times after the shattering of the diaphragm. These calculations are based on the assumptions that the flow is nonviscous and that a plane shock wave is immediately formed which moves into the tube of low pressure while an expansion wave moves into the tube of high pressure. Schardin used the Rankine-Hugoniot relations for the shock fronts and Riemann's relations for the expansion fronts.

By an extension of Schardin's calculations to include reflections and interactions of the waves, as well as the effect of the temperature discontinuity which exists in the flow, a complete time history of the phenomena can be calculated. In order to find the conditions which exist immediately after the shattering of the diaphragm, the method used by Schardin should be briefly reviewed.

In figure 1 is shown the pressure distribution at typical times along constant-area passages which were separated by the diaphragm at $t = 0$. Figure 1(a) shows the pressure distribution along a tube in which a diaphragm separates a pressure p_0 from a lower pressure p_1 . Figure 1(b) shows the pressure distribution along the tube at a time t_b after the diaphragm has been shattered. A shock front is assumed to be propagated towards the region of low pressure and to be compressing the gas at p_1 to an intermediate pressure p_2 . At the same time, a zone of expansion is assumed to be propagated towards the direction of high pressure and to be reducing the pressure p_0 to the same intermediate pressure p_2 . In order to find all the flow quantities existing in the tube at the time t_b , the following assumptions are made:

- (1) The value of γ is constant.
- (2) Velocities are positive in the positive x -direction.
- (3) The tube is of constant cross-sectional area.
- (4) Before the diaphragm is shattered, the temperature in the tube is everywhere the same and the velocity is everywhere equal to 0.
- (5) The flow is nonviscous and involves no transmission of heat.

Immediately after the rupturing of the diaphragm, a temperature contact discontinuity exists in the flow somewhere between the compression front and the expansion front as mentioned previously. This discontinuity also represents an entropy discontinuity, because this discontinuity represents no pressure increment and, hence, no velocity increment. In order to satisfy the assumption that an expansion zone is moving in the

negative x -direction, it now follows from Riemann's work that the velocity u_2 must be in the positive x -direction. Therefore,

$$u_0 + \frac{2}{\gamma - 1} a_0 = u_2 + \frac{2}{\gamma - 1} a_{22}$$

which may be expressed as

$$\frac{u_2 - u_0}{a_0} = \frac{2}{\gamma - 1} \left[1 - \left(\frac{p_2}{p_0} \right)^{\frac{\gamma-1}{2\gamma}} \right] \quad (1)$$

because the process is isentropic and

$$\frac{a_{22}}{a_0} = \left(\frac{p_2}{p_0} \right)^{\frac{\gamma-1}{2\gamma}}$$

Equation (1) expresses the velocity increment across the expansion zone as a function of the pressure ratio across the zone and a_0 , which is a function of the initial temperature.

The velocity increment across the shock front can be expressed in terms of the pressure ratio across the front and a_1 by using the Rankine-Hugoniot relations for a stationary normal shock as follows.

The coordinate system in figure 1(b) can be changed to reduce the shock velocity $W_b = 0$ by expressing the gas velocities on either side of the shock as

$$V'' = u_1 - W_b$$

and

$$V' = u_2 - W_b$$

where V'' is the gas velocity on the low-pressure side of a stationary normal shock and V' is that on the high-pressure side. (See fig. 1(c).) The velocity increment across the shock is then

$$V' - V'' = -M_2 a_2 - (-M_1 a_1)$$

which may be written as

$$\frac{V' - V''}{a_1} = M_1 - M_2 \sqrt{\frac{\frac{2}{\gamma - 1} + M_1^2}{\frac{2}{\gamma - 1} + M_2^2}} \quad (2)$$

where M_1 and M_2 are the Mach numbers on the low-pressure and high-pressure side, respectively, of a stationary normal shock and from the Rankine-Hugoniot relations,

$$\frac{a_2}{a_1} = \sqrt{\frac{\frac{2}{\gamma - 1} + M_1^2}{\frac{2}{\gamma - 1} + M_2^2}}$$

Also, from the stationary-shock relations,

$$M_1 = \sqrt{\frac{(\gamma + 1) \frac{p_2}{p_1} + (\gamma - 1)}{2\gamma}}$$

and

$$M_2 = \sqrt{\frac{(\gamma + 1) \frac{p_1}{p_2} + (\gamma - 1)}{2\gamma}}$$

so that equation (2) may be written as

$$\frac{v' - v''}{a_1} = \frac{u_2 - u_1}{a_1} = \frac{\frac{2}{\gamma - 1} \left(\frac{p_2}{p_1} - 1 \right)}{\sqrt{\frac{2\gamma}{\gamma - 1} \left(\frac{\gamma + 1}{\gamma - 1} \frac{p_2}{p_1} + 1 \right)}} \quad (3)$$

Equation (3) is the expression for the velocity increment across the shock front, for either coordinate system, as a function of the pressure ratio across the front and a_1 . It might be pointed out that the selection of coordinate systems other than the one used herein yields the same relation. (For example, see reference 5.) Equation (3) may be equated to equation (1) because $a_1 = a_0$ and $u_1 = u_0 = 0$ as follows:

$$\frac{p_1}{p_0} = \frac{p_1}{p_2} \left[1 - \frac{\frac{p_2}{p_1} - 1}{\sqrt{\frac{2\gamma}{\gamma - 1} \left(\frac{\gamma + 1}{\gamma - 1} \frac{p_2}{p_1} + 1 \right)}} \right]^{\frac{2\gamma}{\gamma - 1}} \quad (4)$$

Equation (4) can easily be solved graphically for p_2/p_1 . (See fig. 2.) By substituting p_2/p_1 in equation (3), u_2 may be found because a_1 is known from the initial temperature in the tube. Also, w_b may be found from

$$w_b = u_1 - (-M_1 a_1)$$

or the pressure ratio across the shock may be written as a function of the shock speed

$$\frac{p_2}{p_1} = \frac{\frac{2\gamma}{\gamma - 1} \left(\frac{w_b}{a_1} \right)^2 - 1}{\frac{\gamma + 1}{\gamma - 1}} \quad (5)$$

when $u_1 = 0$.

All the conditions in the tube are now known for any time t_b after the shattering of the diaphragm until reflections occur at the ends of the tube. These conditions satisfy the original assumptions of an expansion zone moving in the negative x -direction and a compression shock moving in the positive x -direction, as well as a temperature contact discontinuity ($a_{22} \neq a_2$) moving at the velocity u_2 across which there is no change in pressure or flow velocity. The pressure distribution along the tube is easily found because the shock has moved a distance $W_b t_b$ and the expansion zone AB in figure 1(b) has moved distances of $-a_0 t_b$ and $-(a_{22} - u_2)t_b$ for points A and B, respectively. The expansion zone becomes less steep with time because point A moves faster than point B; whereas a compression shock exists immediately and moves in the positive x -direction because the propagation velocity behind the shock ($u_2 + a_2$) is greater than that ahead (a_1).

Figure 1(d) shows the pressure distribution along the tube at a time t_c after the shock has been reflected from the low-pressure end of the tube and the expansion has been reflected from the other end. The conditions existing after reflection of the shock can be found in a manner similar to that used to obtain equation (3); that is, the reflected shock velocity $-W_c = 0$ can be reduced so that the flow velocities on either side of the shock become (fig. 1(e))

$$V'' = u_2 - (-W_c)$$

and

$$V' = u_3 - (-W_c)$$

The velocity increment across the shock can therefore be expressed in terms of its pressure ratio and a_2 as follows:

$$\frac{V' - V''}{a_2} = \frac{u_3 - u_2}{a_2} = \frac{\frac{2}{\gamma - 1} \left(\frac{p_3}{p_2} - 1 \right)}{\sqrt{\frac{2\gamma}{\gamma - 1} \left(\frac{\gamma + 1}{\gamma - 1} \frac{p_3}{p_2} + 1 \right)}} \quad (6)$$

Because $u_3 = 0$ at the end of the tube, p_3/p_2 can be expressed as a function of p_2/p_1 by combining equation (6) with equation (3) where

$$\frac{a_2}{a_1} = \sqrt{\frac{\frac{2}{\gamma-1} + M_1^2}{\frac{2}{\gamma-1} + M_2^2}}$$

The resulting expression is, for $\gamma = 1.4$,

$$\frac{p_3}{p_2} = \frac{8 \frac{p_2}{p_1} - 1}{\frac{p_2}{p_1} + 6} \quad (7)$$

The shock velocity W_c can be found from

$$-W_c = u_3 - V' = M_3 a_3$$

or

$$-W_c = u_2 - V'' = M_4 a_2$$

where M_3 and M_4 are the Mach numbers on the high-pressure and low-pressure side, respectively, of the reflected shock in stationary coordinates; that is,

$$M_3 = \sqrt{\frac{\frac{\gamma+1}{\gamma-1} \frac{p_2}{p_3} + 1}{\frac{2\gamma}{\gamma-1}}}$$

$$M_4 = \sqrt{\frac{\frac{\gamma+1}{\gamma-1} \frac{p_3}{p_2} + 1}{\frac{2\gamma}{\gamma-1}}}$$

and

$$\frac{a_3}{a_2} = \sqrt{\frac{\frac{2}{\gamma-1} + M_4^2}{\frac{2}{\gamma-1} + M_3^2}}$$

$$= \sqrt{\frac{\frac{\gamma+1}{\gamma-1} + \frac{p_3}{p_2}}{\frac{\gamma+1}{\gamma-1} + \frac{p_2}{p_3}}}$$

All the flow conditions after the reflection of the shock are now known. Schardin's calculations (reference 8) are extended to the reflection of the shock. (See table I.)

In order to extend the calculations to a complete history of the flow inside the tube, the next step is to find the reflection of the expansion zone from the end of the tube. The conditions after total reflection of the expansion are easily found from Riemann's equation where

$$u_4 - \frac{2}{\gamma-1} a_4 = u_2 - \frac{2}{\gamma-1} a_{22}$$

which may be solved for a_4 because $u_4 = 0$ at the end of the tube. The pressure p_4 can then be found from the isentropic relationship

$$\frac{p_4}{p_2} = \left(\frac{a_4}{a_{22}} \right)^{\frac{2\gamma}{\gamma-1}}$$

Because of its thickness, however, the total reflection of the expansion requires a finite time so that the pressure history at the end of the tube during reflection, or the pressure distribution along the axis of propagation between points A and B must be found somewhat differently. This pressure history is obtained by considering the

expansion zone AB to consist of an arbitrary number of small discontinuous isentropic expansion fronts (the usual characteristics method) rather than to be a smooth pressure variation between zone AB. For an illustration of this method, see figure 3 in which the expansion zone AB is assumed to consist of two expansion zones Y and Z which are replaced with isentropic fronts Y and Z. This method is, of course, not rigorous because Riemann has shown that an expansion front cannot remain discontinuous; however, by the choice of small steps the method provides a good approximation. Each front can now be considered individually, and the conditions of u and a on either side of each front can be found from the initial pressure increment assigned the front by

$$u \pm \frac{2}{\gamma - 1} a = \text{Constant}$$

In figure 3, step 2, $p = 1.70$ atmospheres was arbitrarily assigned the region between fronts Y and Z. From the relation $u + 5a = \text{Constant}$ across either front Y or Z (because the fronts are being propagated against the fluid flow) and the adiabatic relations, the value of u and a in this region are found. The speed of each front is assumed to be an average of the values of $u \pm a$ on either side of the front. For this reason, the characteristics method represents an approximation.

The total reflection of the expansion from the end of the tube is obtained by reflection of the small discontinuous expansion fronts individually and by consideration of the subsequent interactions of the reflected with unreflected fronts. In figure 3, step 3, the conditions at the tube end after reflection of front Y are first found by using the relation $u - 5a$ across reflected front Y and by knowing that $u = 0$ at the tube end. The conditions between fronts Y and Z after interaction are next found by using the relationships $u + 5a = \text{Constant}$ across front Z and $u - 5a = \text{Constant}$ across front Y and by obtaining a simultaneous solution for u and a between fronts after the interaction. (See fig. 3, step 4.) The final step is the reflection of front Z from the tube end. (See fig. 3, step 5.)

Because the speeds of all the fronts are known and because all the fronts originate at the diaphragm at $t = 0$, a more convenient method of illustrating the positions of the various fronts in the tube at any time is to plot the time histories as a diagram of x against t as in figure 4 where the expansion is divided into seven fronts. Pressure variations, as a function of time or distance along the tube, are easily taken from such a plot because conditions in each enclosed area are known and are constant throughout the area. In figure 5, the preceding method was used to show the pressure distribution along the tube between points A and B at a time t_p . In figure 6, this method was used to show the variation of pressure at the end of the tube with respect to time at reflection of expansion zone. It can be seen from figures 5 and 6 that the pressure variation inside the expansion front is nonlinear.

Figure 4 shows that, depending on the ratio of the lengths l_L/l_H , the temperature contact discontinuity is overtaken by either the reflected expansion zone or the reflected shock front. Whichever is the case, it can be shown that the pressure ratio of the front is altered after passing through the temperature contact discontinuity which, in turn, generates a second front that propagates itself in the opposite direction. The method used to obtain the conditions which exist after the front has undergone this interaction with the temperature contact discontinuity is similar to the method already used. First, the assumption is made that a second front is generated and travels in the opposite direction from the original front. Then, knowing that there is no velocity increment or pressure increment across the new discontinuity necessitates the finding of four unknown conditions: namely, the pressure and velocity existing in the region between the two fronts, and the two temperatures.

These conditions can be found in the same manner in which the conditions after the shattering of the diaphragm were found, except that the generated front must be assumed to be either a shock or an expansion. After solutions are obtained and the assumption is indicated to be incorrect, a second solution must be obtained. If the interaction under consideration is that of an expansion zone with a discontinuity, the expansion zone must be considered as a number of small fronts (as was the treatment for the reflection of an expansion zone from the end of the tube) in order to obtain a pressure variation with time or distance inside the expansion zone during the interaction. This method is rather laborious and is not required when solving for conditions after the interaction but should be used for an accurate history of events in a diagram of x against t . Interactions of expansion zones and shock fronts with discontinuities have been analyzed by this method, and, in general, the generated front is very weak in proportion to the original front. An interaction of a shock front with a discontinuity is shown in figure 4 in which the generated front is a compression traveling in the opposite direction from the original shock.

In order to be able to find conditions in the tube at any time or position, the one remaining phenomenon which must be considered is an interaction of a shock front with an expansion zone. For this case, the conditions which exist after the interaction is over are again readily found by the methods used for finding the conditions after the shattering of the diaphragm. The only assumption that satisfies a solution of this interaction is one in which a shock and an expansion are propagated in the same direction after the interaction as before the interaction and in which the flow between the two fronts is reversed in direction. The values of u , a , and p , which exist between the fronts after interaction, can be obtained by making this assumption and by obtaining simultaneous solutions of the shock equations and the isentropic-front equations. The expansion, however, must be considered as a number of small fronts and the method must be applied the same number of times if a pressure variation of time or distance is to be obtained during the interaction. An interaction between a shock front and an expansion zone is shown in figure 4.

By use of the methods which have been discussed it is possible to determine all the subsequent phenomena and to obtain the complete pressure history in the tube at any point in the tube or a complete pressure distribution along the tube at any time after the diaphragm is shattered. The assumptions of nonviscous flow of a gas which has a constant value of γ and which involves no heat transmission should be valid in many cases. However, for passages of very small cross section or long length and for pressure variations involving large temperature variations, these assumptions would undoubtedly lead to incorrect results. The method which has been presented can, in many cases, be greatly simplified for small pressure variations. In these cases the shock can be treated as an isentropic pressure front, and Riemann's relations, rather than the shock relations, can be used with very little error. Also, the expansion zone need not be broken into a large number of weaker fronts; usually two or three will suffice.

EXPERIMENTAL METHOD

A diagrammatic sketch and photographs of the apparatus are shown in figures 7 and 8, respectively. A description of the design and function of the instrumentation, much of which was developed specifically for these tests by the Langley Instrument Research Division, was prepared by Mr. F. Delpino and is given in the appendix.

The apparatus in which the waves were produced consisted of four passages of constant internal cross-sectional area which could be connected together in any sequence by means of clamps and by mating flanges to form one long passage with smooth concentric inner surfaces. The internal dimensions were everywhere 3 inches wide by 3 inches high.

The walls were fabricated from $\frac{3}{16}$ -inch brass stock by brazing the joints along the outside surface of the passage. The four sections included a section 8 inches long which contained a solenoid-actuated trigger used to puncture the diaphragm. (See fig. 7(c).) Also included was a 24-inch section, a 48-inch section, and a $24\frac{1}{2}$ -inch section, which was equipped with two pairs of glass windows of such dimensions that the full 3-inch height of the passage for a distance of 6 inches along the passage could be photographed from either pair of windows. The glass windows were mounted in such a manner that the inner surfaces of the glass were flush with the inner surfaces of the passage with gaskets between the joints to prevent leakage of air. Each section of passage was equipped with two small static-pressure orifices (0.04-inch diameter), one which could be connected to a pressure gage and the other, to a source of pressure or vacuum. At the positions shown in figure 7(a), each section was equipped with tapped holes along the top of the passage which could accommodate either a blank plug screwed in flush with the inner surface or a plug in which the pressure-measuring instrument was mounted flush with the surface as shown in figure 7(b). Three metal end plates were

provided of thicknesses of $3/16$ inch, $3/8$ inch, and $11/16$ inch, each of which could be clamped to the end of any section of passage.

In all the tests, the 8-inch trigger section, the 24-inch section, and the $3/8$ -inch end plate were clamped together to form what is called the high-pressure chamber. The low-pressure chamber then consisted of either or both of the remaining two sections in addition to the $11/16$ -inch end plate. In this manner three different lengths of low-pressure chamber were available in four possible combinations of section - that is, one $24\frac{1}{2}$ inch, one 48 inch, and two $72\frac{1}{2}$ inch - in which the glass section could be at either end. All the clamped joints between sections and between a section and an end plate were equipped with rubber gaskets of such dimensions that the inner edges were flush with the inner surfaces of the passages. The trigger was equipped with a sliding pressure seal and a soft rubber cushion to damp out mechanical vibration. (See fig. 7.) The blank plugs and instrument plugs were equipped with rubber gaskets. The diaphragm used to separate the high-pressure chamber from the low-pressure chamber consisted of from one to four thicknesses of a special paper, depending on the pressure difference between the two chambers, and was inserted in this joint along with a rubber gasket before clamping. The particular paper used, American Blueprint Co. Inc., No. 45D, Type 2, tracing paper, was selected after many preliminary trials because of the following favorable characteristics: very little stretching under tension; minimum porosity and hence minimum leakage of air through the paper before puncturing; and, finally, disintegration into small pieces when punctured rather than simply tearing into four pie-shaped pieces. The pressure-measuring instrument was a commercial unit consisting of an ammonium dihydrogen phosphate piezoelectric crystal mounted in a metal case of $5/8$ -inch diameter and 1-inch length. The electrical characteristics of this instrument are described in the appendix. This instrument has the following desirable characteristics for this type of test: rugged construction, high acoustic impedance, high sensitivity, and no cavity resonance.

Before each series of tests, the high-pressure and low-pressure chambers were clamped together without a diaphragm and the entire unit was checked for air leakage. Before each test, the small bits of paper left in the chambers from the preceding test were blown out with an air hose. After a new diaphragm was clamped between the high-pressure and low-pressure chambers, the pressure in each chamber was adjusted to the desired values and read from calibrated pressure gages to an accuracy of 0.1 pound per square inch. The pressures were held steady for a few minutes before each test so that the temperatures could come into equilibrium with the room temperature. Because the gage leads and pressure-supply leads were connected to the apparatus through small orifices and because the duration of the test was only a few milliseconds,

the small amount of flow induced through these orifices during the test were believed to be of no consequence.

Photographs of the flow were taken with a conventional schlieren system which included two parabolic front-surfaced mirrors of 6-inch diameter and a high-voltage-spark light source which was synchronized with the diaphragm burst as described in the appendix. Measurements of the absolute magnitude of the shock speed before its reflection from the end of the low-pressure chamber were made as described in the appendix.

Preliminary tests were made by using a setup of smaller dimensions than the one previously described. These tests were made principally in order to develop the instrumentation. Additional preliminary tests were made by using the apparatus described in order to determine the effects of the following objectionable conditions on the pressure records:

- (1) Air leakage or air cavity around the crystal unit
- (2) Mounting of the crystal unit in rubber instead of the Micarta mount shown in figure 7(b)
- (3) Mechanical vibration caused by the solenoid-actuated trigger
- (4) Failure of the crystal unit to be perfectly flush with the inner surface of the passage or end plate
- (5) Failure of the diaphragm to disintegrate after bursting
- (6) Mechanical vibration of the end plates set up by the reflection of the shock waves

Before the effect of these conditions on the test results are discussed, the method of interpreting the test records should be discussed. As pointed out in the appendix, the test records are essentially a plot of the voltage developed by the crystal unit as a function of time provided that proper electrical instrumentation is used. If, therefore, the pressure sensitivity of the crystal unit is known (that is, the voltage output as a function of pressure change at the crystal), the test results can then be compared with theory by comparing the theoretical and experimental pressure-time plots. The theoretical pressure-time plot for any position of the crystal unit can be taken from plots such as those shown in figures 9(a) to 9(c), which were obtained for a pressure ratio p_0/p_1 of 2.0 for the three lengths of low-pressure chamber, by using the methods outlined previously and by assuming the fluid to be air ($\gamma = 1.4$). In figure 10, the theoretical pressure-time plots are shown as dash lines for a number of different locations and lengths of low-pressure chamber, all for p_0/p_1 of 2.0.

With the theoretical pressure-time plot known, the effects of the objectionable conditions previously listed were experimentally studied and the results of these preliminary tests are as follows:

(1) Records were taken with and without air leakage and an air cavity around the crystal unit. Comparison of the records indicated that a sharp fall of the trace occurred immediately following a pressure rise at the crystal when leakage and air cavity were present.

(2) Records were taken with the crystal unit mounted in rubber and were compared with records taken with the unit mounted in the Micarta mount shown previously. Oscillations of the trace on the records taken with the rubber mount occurred following a sharp compression. These oscillations indicated that the crystal was oscillating mechanically at the frequency of the rubber mount.

(3) Records were taken with no pressure difference across the diaphragm, and a comparison was made of the trace obtained with and without a soft rubber cushion on the trigger mechanism shown previously. The mechanical vibration caused by the trigger hitting the stop on the side of the passage was found to be substantially eliminated by the rubber cushion.

(4) Records taken with the surface of the crystal unit not flush with the inner surface of the passage or end plate indicated that the trace was distinctly altered because of the waves reflected from the crystal edges in this condition.

(5) Records were taken of bursts in which more thicknesses of paper diaphragm were used than necessary, in which case the burst was more a tearing of the paper than a disintegration of the paper into tiny pieces. These results indicated that in cases where the paper did not disintegrate the rise of the trace as a result of a compression was more gradual and was followed by oscillations of the trace, probably a result of small waves behind the compression front caused by poor air flow past the remaining part of the diaphragm.

(6) On all records taken with the crystal unit in the end plates, a rather violent oscillation of the trace would always occur following a compression. This oscillation would not occur following an expansion, nor would it occur for either case if the crystal unit was mounted in the side of the passage. Also, the use of thicker end plates increased the frequency of this oscillation but had little effect on its amplitude. The addition of a 6-pound weight onto the plug in which the crystal was mounted (fig. 7(b)) would decrease the frequency of oscillation for a given end-plate thickness. In all cases the rise of the trace due to the compression was reproduced (for a given pressure) if measured to the mean of this oscillation. The oscillation was a result of mechanical vibration of the end plate excited by the sharp pressure change in the compression and was extremely difficult to eliminate.

The qualitative nature of all these effects can be predicted from general unsteady-flow theory; however, it was desired to determine the order of magnitude of the effects before analyzing the records. As a

result of these preliminary tests, the standard configuration for all subsequent tests, unless otherwise noted, incorporated a Micarta crystal unit mount as shown in figure 7(b), a soft rubber cushion on the trigger as shown in figure 7(c), an $\frac{11}{16}$ -inch-thick end plate on the low-pressure chamber, and - as pointed out in the appendix - a 100-micromicrofarad condenser across the crystal as well as a 47-kilocycle filter in the preamplifier circuit.

RESULTS AND DISCUSSION

A large number of test records were taken at various crystal positions and with the three different low-pressure-chamber lengths. Records were taken over a range of pressure ratio p_0/p_1 across the diaphragm from 1.3 to 2.5 where p_1 , the pressure in the low-pressure chamber, was equal to 1 atmosphere or $1/2$ atmosphere. Typical pressure records which were obtained are shown in figure 11.

Before the experimental records can be superimposed on a given pressure-time scale for comparison with theory, it is necessary to know the voltage output of the crystal unit as a function of the pressure change experienced by the crystal unit. This pressure sensitivity of the crystal unit was found experimentally by plotting all the voltage changes as measured from the test records as a function of the pressure changes experienced by the crystal as predicted by the theories previously outlined. In figure 12 and table II are shown the results of these voltage measurements, along with the positions on the test records at which voltage measurements were taken. These data indicate that, with only a very small scatter of points, a straight line can be drawn through the points starting from zero; that is, the output of the crystal unit is a linear function of the pressure change at the crystal, within the range of pressures shown. As shown in figure 13, the voltage measurements E were taken from the test records by first drawing a straight line (shown as a dash line) through the part of the trace immediately following either an expansion or compression and extending it to the point in time at which the voltage change began. This line corrects the measurement for the slight fall of the trace towards zero voltage inherent in the crystal and electrical circuit as pointed out in the appendix. No significant difference was noted among records taken with a number of crystals all of the same model type.

Because the abscissa in figure 12 is the theoretical pressure difference experienced by the crystal unit for a given p_0/p_1 across the diaphragm, it was necessary to determine experimentally if the absolute magnitude of this pressure difference was that predicted by theory. In order to do this without making a pressure measurement, the value of the shock speed W_b was experimentally measured (see appendix) and the pressure p_2 was calculated from equation (5), p_1 and a_1

being known. The results of these measurements are shown in figure 2, where it can be seen from the measured values of p_2/p_1 that the actual values of Δp are only a few percent lower than the theoretical values. The use of Δp to calculate the shock speeds gave values only a fraction of a percent lower than theoretical shock speeds.

The experimental pressure-time records for $\frac{p_0}{p_1} = 2.0$ were superimposed on the theoretical pressure-time plots and are shown as solid lines in figure 10. In figure 10 the pressure scales (that is, voltage scales) for the theoretical trace were taken from figure 12, and the test records were superimposed by tracing directly from the records on a light table. The time scales and voltage against trace deflection scales were taken from the timing frequency traces and the alternating-current voltage traces on the test records.

Figure 10 shows that the agreement between the theoretical and experimental pressure-time plots is very close. The slight departure which is shown is seen to be mainly due to the fall of the trace towards zero voltage, previously mentioned as a condition inherent in the electrical circuit. This fall was measured (see appendix) and was about $1\frac{1}{2}$ percent of the voltage per millisecond. Although this correction was not made in figure 10, the agreement would be still closer if the correction were made.

Schlieren photographs taken by using the $24\frac{1}{2}$ -inch low-pressure chamber and by using the $72\frac{1}{2}$ -inch low-pressure chamber with the glass section at the end plate are shown in figure 14. As a result of the schlieren photographs, shock-speed measurements, and pressure records, a number of interesting comparisons can be made between the experimental results and the theoretical predictions which were based on one-dimensional unsteady flow.

The first assumptions made were that the flow was frictionless and that a plane compression shock is immediately formed after the shattering of the diaphragm. In figure 12, points taken at crystal locations ranging from $7\frac{1}{2}$ inches from the diaphragm up to $72\frac{1}{2}$ inches from the diaphragm indicate that the shock does not exhibit any measurable attenuation within the scatter of the points (less than 1 percent of Δp). This assumption is further confirmed by the pressure-time records in figure 10 and the shock-speed measurements in figure 2 where attenuation would show up as a change in shock speed and thereby cause disagreement with the theoretical pressure-time plot. The schlieren photographs and pressure-time records show that the compression is not immediately one dimensional and discontinuous but that it becomes so very rapidly.

At $7\frac{1}{2}$ inches from the diaphragm the schlieren photographs and pressure-time records (figs. 14(a), 14(b), and 10(d)) indicate that the compression has a definite thickness; however, the schlieren photographs and

pressure-time records taken at 17 inches and $24\frac{1}{2}$ inches, respectively, (figs. 14(d), 10(a), 10(b), and 10(c)) indicate that the shock is very sharp after this length of travel. This rapid steepening is to be expected from theoretical considerations because for this p_0/p_1 the value of $u + a$ behind the shock is appreciably larger than that ahead of the shock (1462 fps as compared with 1126 fps). It cannot be definitely established from these results why the shock is not immediately plane and discontinuous, but it might be due to either an initial shock curvature because of the bowed diaphragm (in which case there would be oblique reflections from the walls trailing the shock) or due to the finite time required for the shattered pieces of diaphragm to spread out from the point of rupture.

The next assumption made was that the temperature contact discontinuity represented no pressure (that is, velocity) increment. The record in figure 10(d) shows that no pressure change is recorded at the point (about 1.75 milliseconds after the compression) where the discontinuity passes the crystal.

Finally, the theoretical method is based on the assumption that the diaphragm instantaneously disappears such that not only are plane discontinuous compression and expansion fronts generated but a plane temperature contact discontinuity is also generated. The schlieren photographs and pressure-time records, however, show that this assumption is not the case experimentally. The pressure-time records show that the expansion zones are slightly thicker than expected from theory (fig. 10), and the schlieren photographs and pressure-time records show that the temperature contact discontinuities appear to be a thick region of mixing in the flow. Figure 14, in which the reflected shock is being propagated through the temperature contact discontinuity, shows that some distortion of the shock is evident, probably a result of the unequal temperature distribution. From figure 10(a), a gradual rise occurs where a sharp compression was expected theoretically as a result of the interaction of this reflected shock with the temperature contact discontinuity.

A possible explanation for these results might be that in the case of an expansion which is not initially plane because of the diaphragm bowing, oblique reflections of the expansion from the wall would not theoretically catch up with the expansion. Also the temperature contact discontinuity, when not initially plane, would become a vortex in the flow because of its entropy variation.

The pressure records have previously shown that the reflection of the shock from the end plates gave rise to mechanical oscillation of the end plates. The pressure waves generated as a result of this oscillation can be seen in figure 14 to be trailing the reflected shocks.

CONCLUDING REMARKS

Experimental pressure-time measurements, shock-speed measurements, and schlieren photographs have been presented and the results indicate that the unsteady flow generated experimentally conforms accurately with the flow defined by one-dimensional, nonviscous, unsteady-flow theory. The agreement of experimental measurements with theoretical calculations was considered excellent for flows involving pressure disturbances (including compression shocks or expansion zones), temperature-contact discontinuities, and reflections or interactions of these quantities. Slight discrepancies were observed in the correlation of the data and were believed to be introduced by failure to generate exactly the idealized type of flow assumed in the theory. The successful recording of the unsteady flow properties was largely attributed to the special equipment developed for this purpose.

Langley Aeronautical Laboratory

National Advisory Committee for Aeronautics

Langley Air Force Base, Va., March 17, 1949

APPENDIX

INSTRUMENTATION

Apparatus for Measuring and Recording Pressures

Crystal, preamplifier, and filter.— The theoretical shape of the pressure history to be recorded is shown in figure 10. The steepness of the leading edge and the flatness of the constant-pressure portion of the record are dependent upon the response characteristics of the crystal and preamplifier combination. The crystal and preamplifier combination required to reproduce the pressure history shown is essentially one with a very low-frequency response as well as a high-frequency response.

The pressure-measuring element used was a Massa M-101 piezoelectric pressure pick-up. The first records taken showed that the high-frequency response of the crystal was sufficient to reproduce satisfactorily the steep leading edge but that poor low-frequency response resulted in a noticeable drop in the output during the time of constant pressure. The open-grid cathode-follower preamplifier circuit shown in figure 15 was developed to present a maximum impedance to the crystal unit in order to obtain low-frequency response. The addition of the 100-micromicrofarad condenser across the input further increased the low-frequency response without noticeably affecting the steepness of the wave front.

Figure 16 shows the input-output voltage of the preamplifier alone. Negative input voltages are seen to have resulted in distortion which made it necessary to bias the grid positively when recording calibrating voltages if a sine-wave voltage was used. The grid-to-cathode resistance is shown to be effectively infinite until the grid is 14 volts positive so that leakage of the piezoelectric charge was due only to the internal resistance of the crystal itself. Records of crystal leakage were made by impressing a direct-current voltage momentarily across the crystal when in combination with the preamplifier and 100-micromicrofarad condenser and by recording the exponential decay of the voltage output of the preamplifier; the procedure was then repeated without the crystal in the circuit. The time constant of the crystal was found to be 55 milliseconds; that is, two-thirds of the charge on the crystal was dissipated in 55 milliseconds, about $1\frac{1}{2}$ percent per millisecond. In order to maintain this time constant, the crystal must be dehydrated after each day's use by storing it in a flask containing a dessicant. The slope of the trace during the constant-pressure portion of the records shown in figure 10 illustrates the very small leakage occurring during this time.

The appreciable amplitude of hash observed on the record shown in figure 17(a) was generated by the crystal's resonating at its natural frequency of about 47 kilocycles after being excited by the steep wave front. Satisfactory attenuation of the resonant frequency was obtained by the use of filters as is shown by the record of figure 17(b) which

was taken under conditions similar to those for figure 17(a) except that a filter was used. The filter was constructed in accordance with the diagram shown in figure 18 with parts that were accurate to within ± 1 percent and functioned satisfactorily with the different crystals used during the investigation. With the filter in the circuit some attenuation of frequency components above 5000 cycles can be expected; however, the rise time at the leading edge would be the only part affected in these records.

Because the preamplifier output for the range of pressures covered in these tests was of the order of 10 volts, amplification, in addition to that of the oscilloscope amplifier, was not needed.

Recording apparatus.— At first, records were made by photographing a four-beam commercially constructed oscilloscope. The four beams made it possible to record simultaneously the pressure history, a $\frac{1}{1000}$ -second timer, a 1000 cycle calibrating voltage, and a reference line. Because defocusing at high intensities masked many details in the records made with the four-beam oscilloscope, it was replaced with a single-beam oscilloscope of higher resolution that gave records of more detail and higher contrast. When this single-beam oscilloscope was used, the reference line and calibrating voltages were recorded immediately preceding a test on the same film record. Calibration indicated that the spot deflection on the oscilloscope varied linearly with input voltage to the preamplifier until saturation of the preamplifier.

Moving film and no sweep of the spot, rather than single sweep with stationary film, was chosen as the method of photographing the record. Records were taken with an NACA drum camera using an $f/2.0$ lens and orthochromatic film $2\frac{7}{16}$ -inches wide. This camera consists of a drum $16\frac{1}{4}$ inches in circumference rotated at 3600 rpm by means of a synchronous motor so that the film speed is 0.95 ± 1 percent inch per millisecond. The shutter was set for $1/50$ second and was synchronized with the drum of the camera and solenoid trigger on the experimental apparatus as described in the following section.

Synchronizing circuit.— Figure 19 shows a block diagram of the synchronizing circuit. A small bar magnet cemented on the film drum generated a trigger signal as it passed a coil mounted on the drum-case lid. The trigger signal caused the shutter solenoid to be energized which in turn released the shutter. After a delay of a few milliseconds, the external solenoid for actuating the diaphragm-rupturing trigger on the experimental apparatus was also energized. Film was loaded on the drum so that it began and ended at the bar magnet, thereby establishing a definite time relation between the trigger signal and the instant the beginning of the record passed the lens. The shutter was set for $1/50$ second or one complete revolution of the film drum.

The pulse-delay circuit (fig. 20) which synchronized the schlieren apparatus with the diaphragm burst was actuated by a crystal near the diaphragm and was set to give the delay required for the shock to travel from the crystal to the glass section of the experimental apparatus. The delay was set by means of a 10-turn helical potentiometer which was calibrated by use of a Potter interval timer. It was determined that the delay interval could be reset within ± 10 microseconds consistently. The pulse-delay circuit was connected to the socket of existing spark equipment used for schlieren photography so that the output voltage pulse fired a thyratron which was in series with the primary winding of an ignition coil. The ignition coil in turn fired a series pilot gap which set off the main spark gap.

Apparatus for Recording Shock Speed

The speed of the shock was determined by measuring the interval between the time the shock passed the window of the experimental apparatus and the time it reached the end plate by means of the following arrangement: A sine wave of 10,000 cycles per second was impressed on the vertical axis of an oscilloscope to provide a time scale, and two pulses representing these two positions of the shock were applied to the horizontal scale. One of these pulses was the variation in the output of a 931 photomultiplier tube caused by the bending by the shock wave of a beam of light which emerged from a slit 0.020-inch wide and 1-inch high, passed through the windows of the experimental apparatus at a point $19\frac{19}{32}$ inches from the end of the low-pressure chamber, and activated the photomultiplier tube. (The light from the slit was cut off from the photomultiplier by a knife-edge when no shock was present.) The other pulse was the output of a crystal caused by the impact of the shock on the end plate of the $72\frac{1}{2}$ -inch low-pressure chamber to which the crystal was attached. The trace on the oscilloscope was photographed with the drum camera synchronized to the diaphragm burst as previously described. The sine-wave frequency was accurate to within one part in 100,000 and the outputs of the photocircuit and crystal (without preamplifier and filter) were sharp enough for the departure of the spot from the sine pattern to be read to about 1 microsecond in 1200. Six records were taken at each point shown in figure 2 and the maximum scatter of the records at each point was less than ± 1 microsecond in about 1200.

REFERENCES

1. Seippell, Claude: Pressure Exchanger. U. S. Patent Office 2,399,394, Pat. April 30, 1946.
2. Ferri, Antonio: Esperienze su di un biplano iperacustico tipo Busemann. Atti di Guidonia, no. 37-38, 1940, p. 334.
3. Riemann, B.: Ueber die Fortpflanzung ebener Luftwellen von endlicher Schwingungsweite. Abh. der Koniglichen Gessellschaft der Wissenschaften, vol. 8, 1858-59, pp. 43-65.
4. Hess, Robert V.: Study of Unsteady Flow Disturbances of Large and Small Amplitudes Moving through Supersonic or Subsonic Steady Flows. NACA TN 1878, 1949.
5. Sauer, R.: Theory of Nonstationary Gas Flow - II. Plane Gas Waves with Compression Shocks. Translation No. F-TS-758-RE, Air Materiel Command, U. S. Army Air Forces, Sept. 1946.
6. Rayleigh, (Lord): Aerial Plane Waves of Finite Amplitude. Scientific Papers, vol. V, Cambridge Univ. Press, 1912, pp. 573-610.
7. Courant, R., and Friedrichs, K. O.: Supersonic Flow and Shock Waves. Pure and Appl. Math., vol. 1, Interscience Publishers, Inc., New York, 1948.
8. Schardin, H.: Bemerkungen zum Druckausgleichsvorgang in einer Rohrleitung. Physik. Zeitschr. Jahrg. 33, Nr. 2, Jan. 15, 1932, pp. 60-64.

TABLE I
THEORETICAL CALCULATIONS OF UNSTEADY FLOW VALUES

[Calculated for $T_0 = T_1 = 67.4^\circ \text{F}$]

$\frac{u_2}{a_0}$	$\frac{p_2}{p_0}$	$\frac{u_2 - a_{22}}{a_0}$	$\frac{W_b}{a_0}$	$\frac{p_2}{p_1}$	$\frac{p_1}{p_0}$	$\frac{p_2 - p_1}{p_0}$	$T_0 - T_{22}$ ($^\circ\text{F}$)	$T_2 - T_1$ ($^\circ\text{F}$)	$\frac{W_c}{a_0}$	$\frac{p_3}{p_2}$	$\frac{p_3}{p_0}$	$\frac{p_3 - p_2}{p_0}$	$T_3 - T_2$ ($^\circ\text{F}$)
a0.10	0.868	-0.880	1.062	1.149	0.756	0.112	20.9	21.3	-0.981	1.147	0.994	0.126	21.8
.1445	.816	-.828	1.089	1.223	.667	.148	29.8	30.7	-.9755	1.216	.989	.1755	32.0
.15	.808	-.820	1.094	1.230	.657	.151	31.2	32.2	-.974	1.222	.988	.180	33.2
a.20	.751	-.760	1.127	1.316	.571	.180	41.4	43.3	-.966	1.302	.979	.227	45.0
.248	.701	-.703	1.159	1.402	.500	.201	51.0	54.2	-.9612	1.380	.968	.266	57.1
.25	.698	-.700	1.161	1.406	.497	.202	51.5	54.6	-.961	1.384	.967	.268	57.3
a.30	.649	-.640	1.196	1.502	.432	.217	61.4	66.2	-.955	1.469	.953	.304	70.0

^aValues taken from reference 8.

NACA

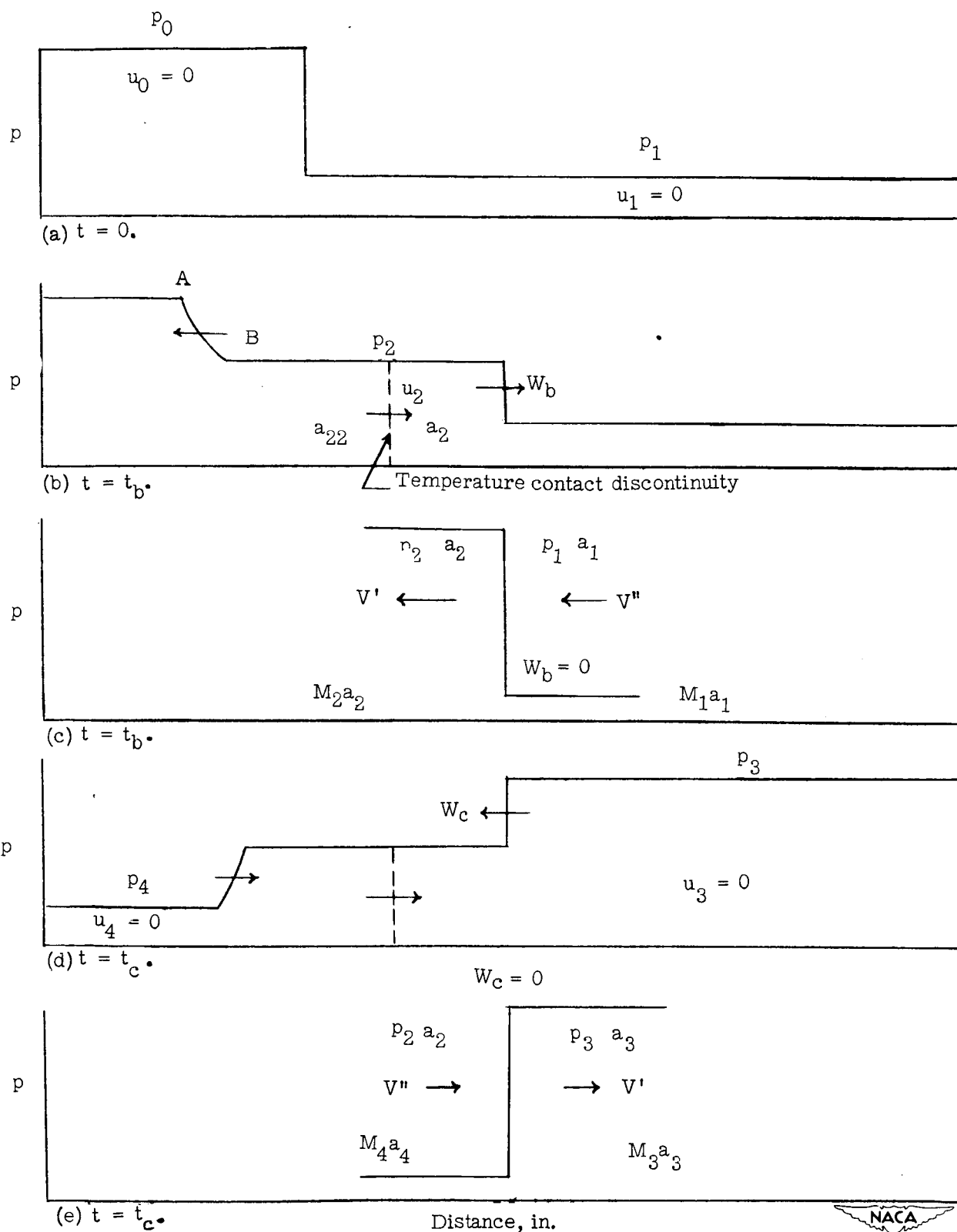


Figure 1.— Pressure distribution at typical times along constant area passages which were separated by diaphragm at $t = 0$.

○ Value of p_2/p_1 calculated from equation (5) and measurements of W_b

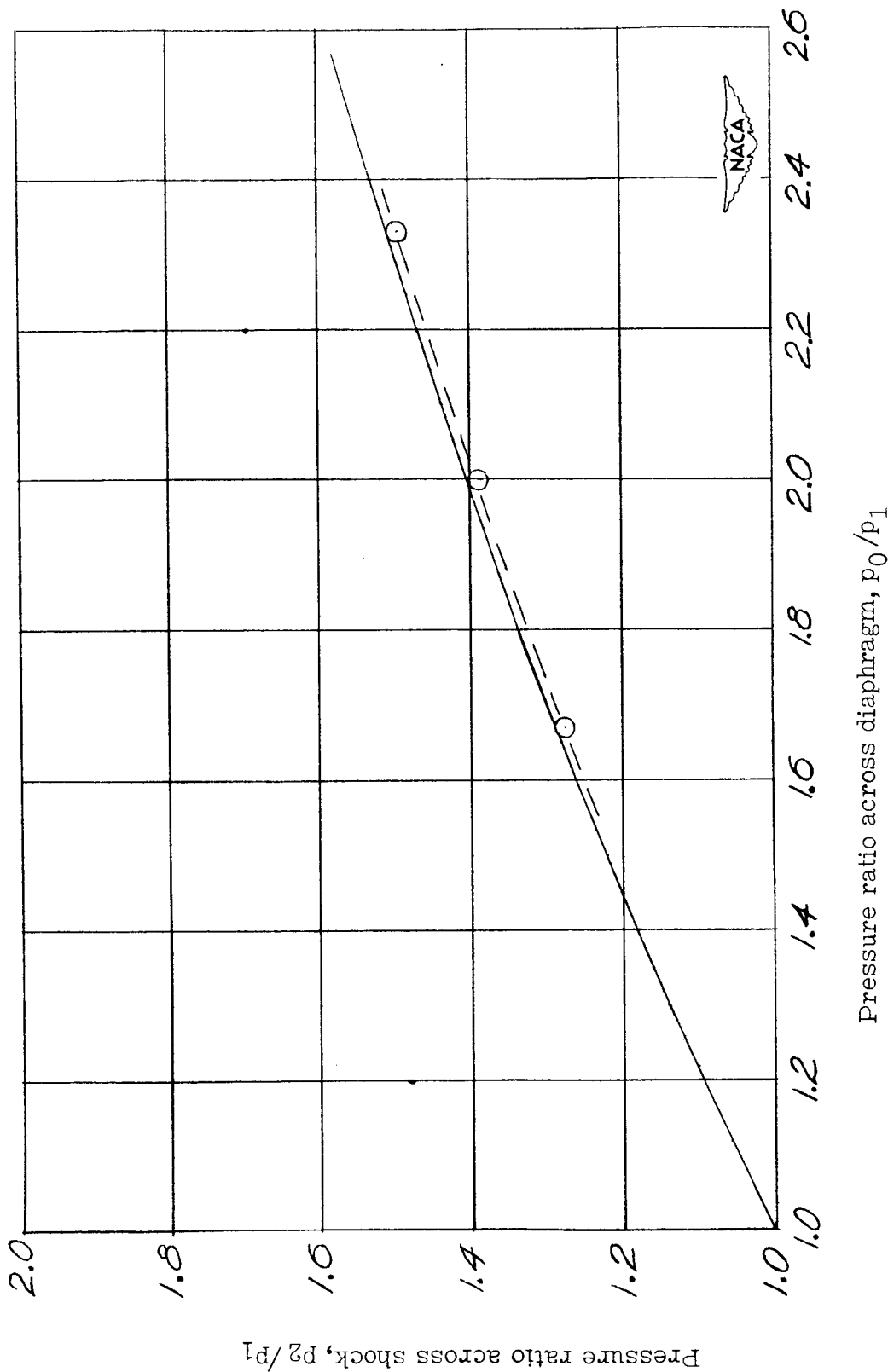
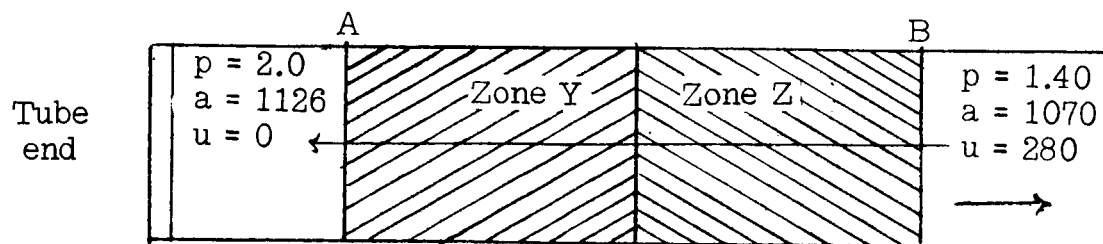
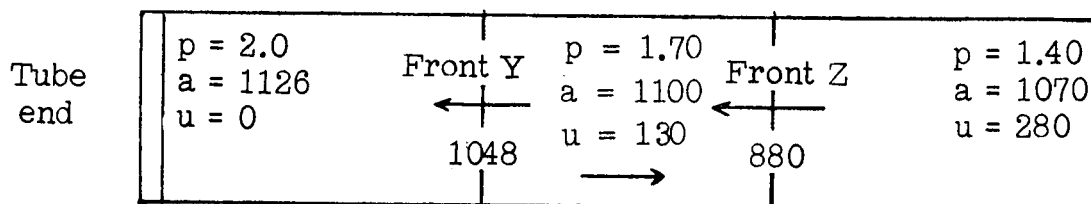


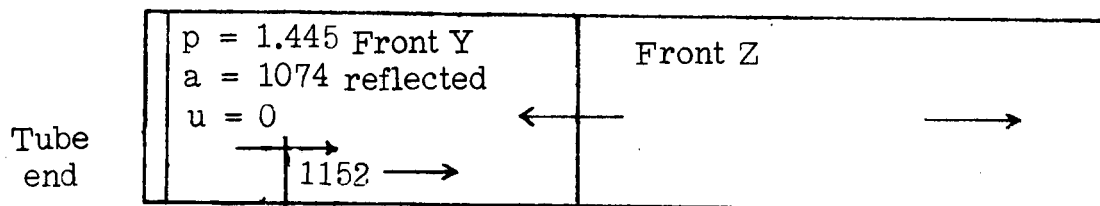
Figure 2.- Theoretical and experimental pressure ratio across compression shock before reflections as function of pressure ratio across diaphragm before bursting. $a_0 = a_1$.



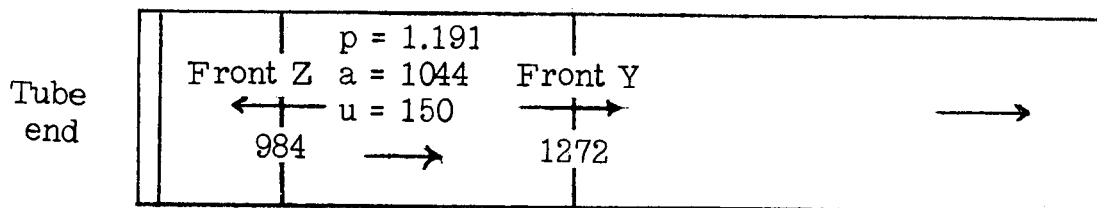
Step 1.- Zone AB considered as zones Y and Z.



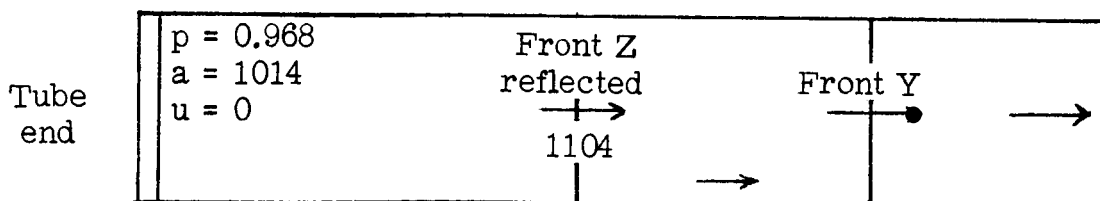
Step 2.- Zones Y and Z replaced with fronts Y and Z.



Step 3.- After reflection of front Y.



Step 4.- After interaction of reflected front Y and front Z.



Step 5.- After reflection of front Z.

Figure 3.- Illustration of treatment of expansion zone by considering the expansion zone as a number of discontinuous expansion fronts. The values shown were obtained by assuming the fluid to be air ($\gamma = 1.4$).

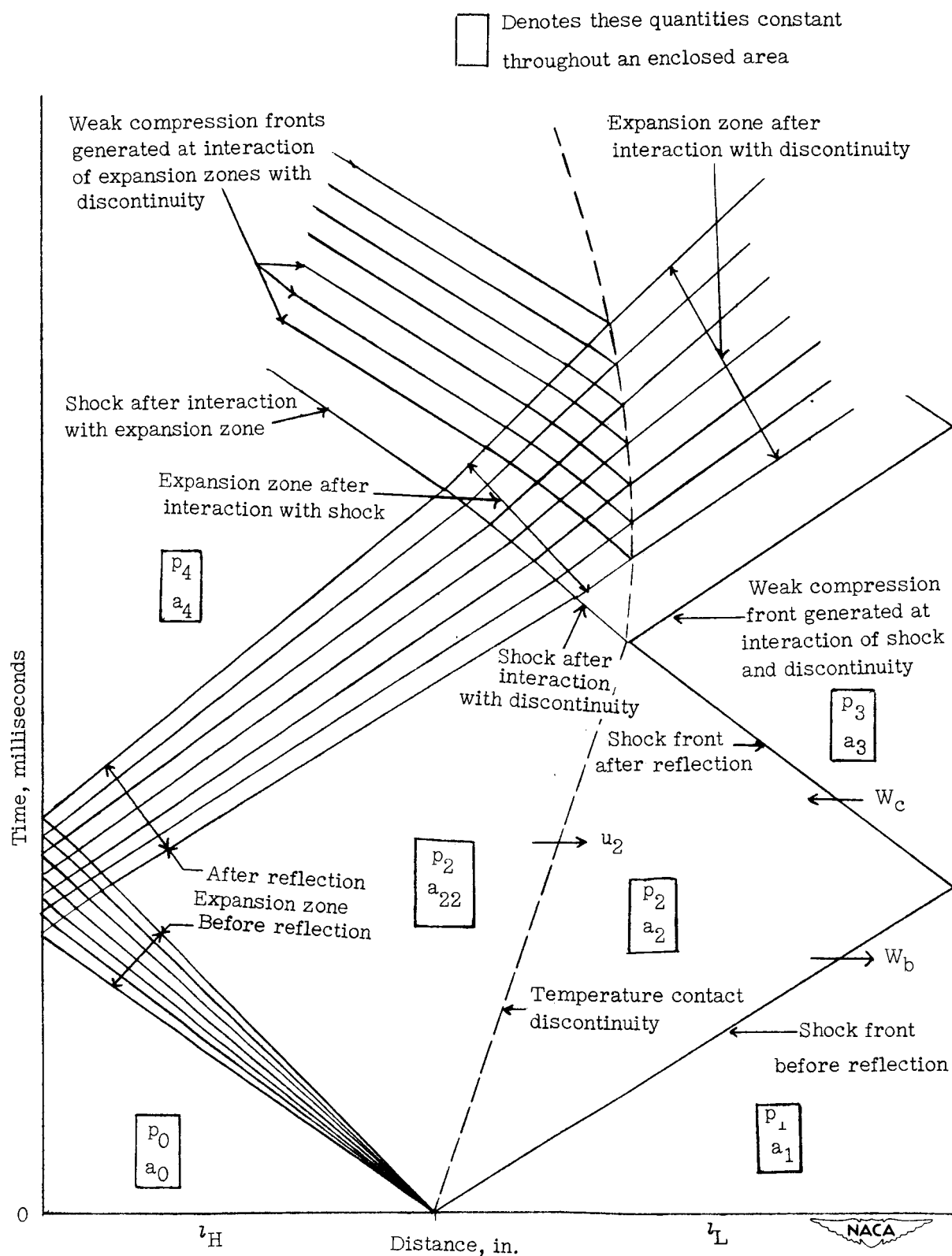


Figure 4.— Typical diagram of x against t showing position histories of unsteady flow quantities following diaphragm burst in constant area passages. $a_0 = a_1$.

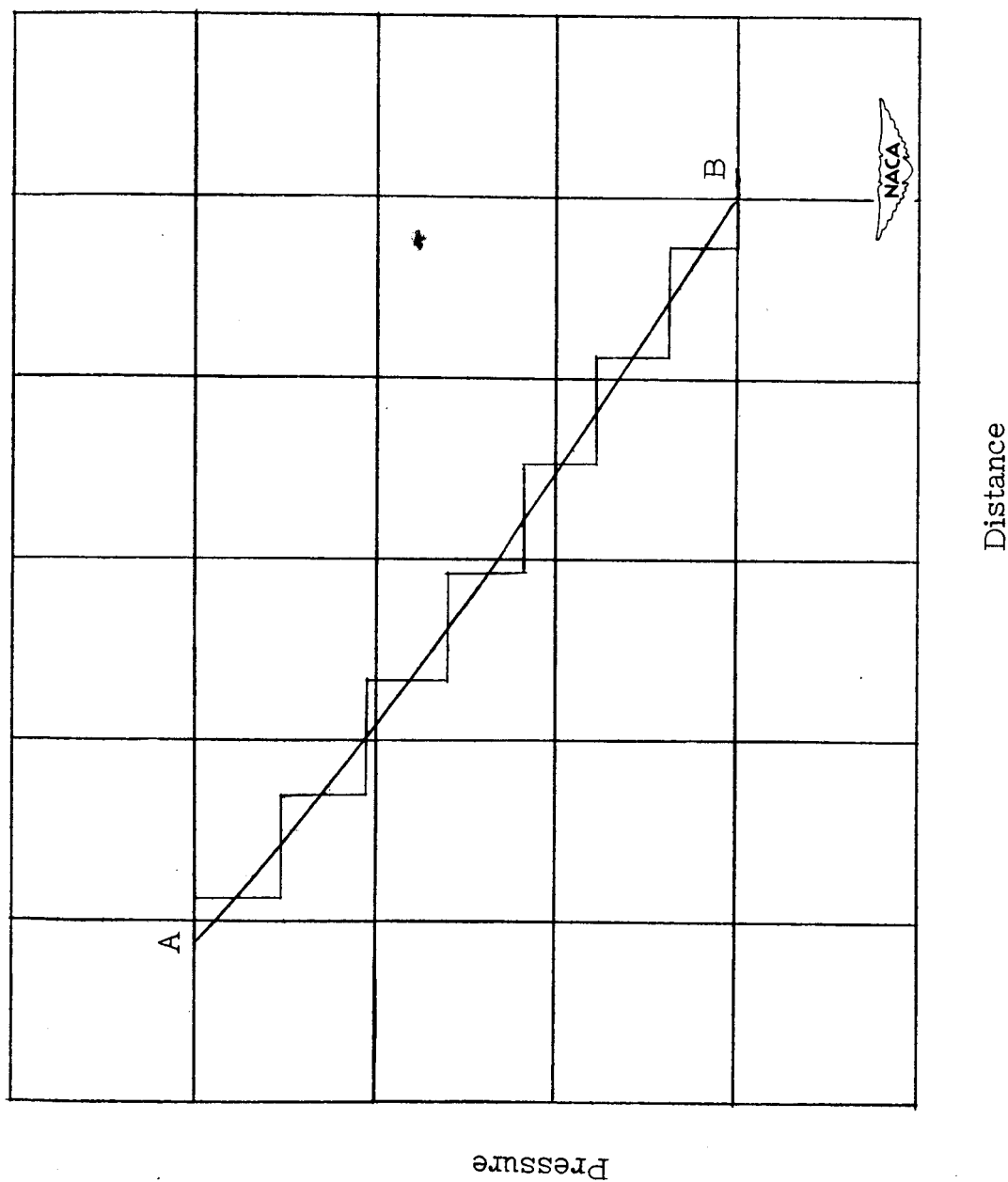
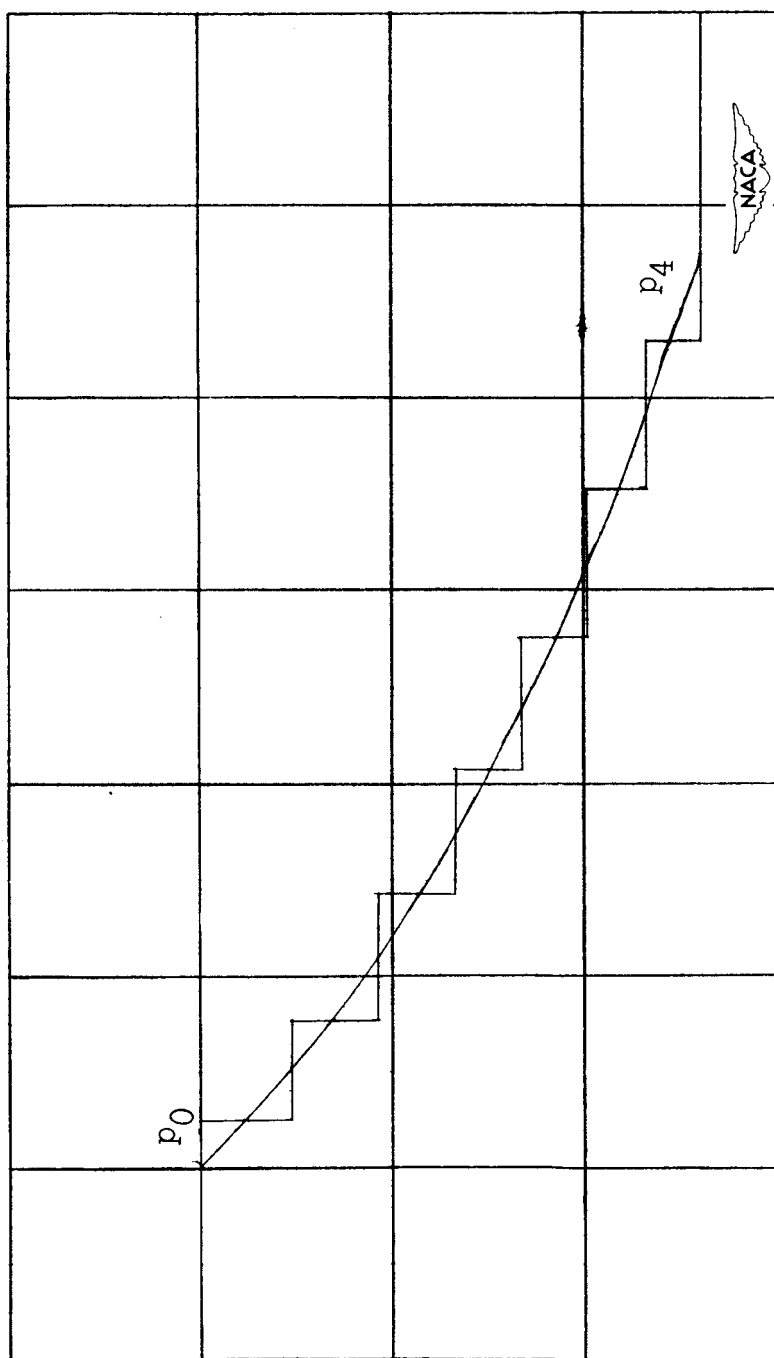
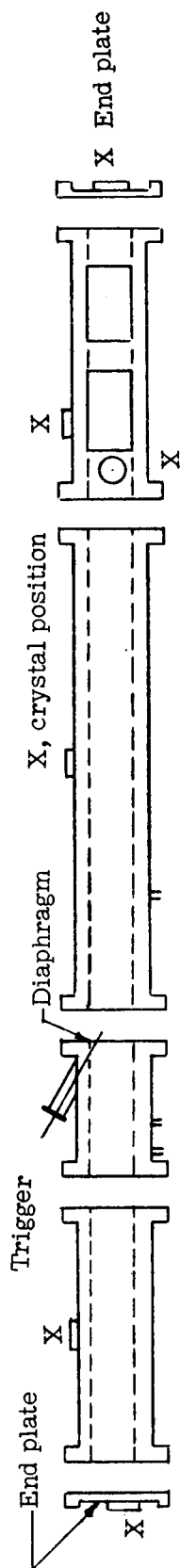


Figure 5.- Pressure distribution along axis of propagation of expansion zone.

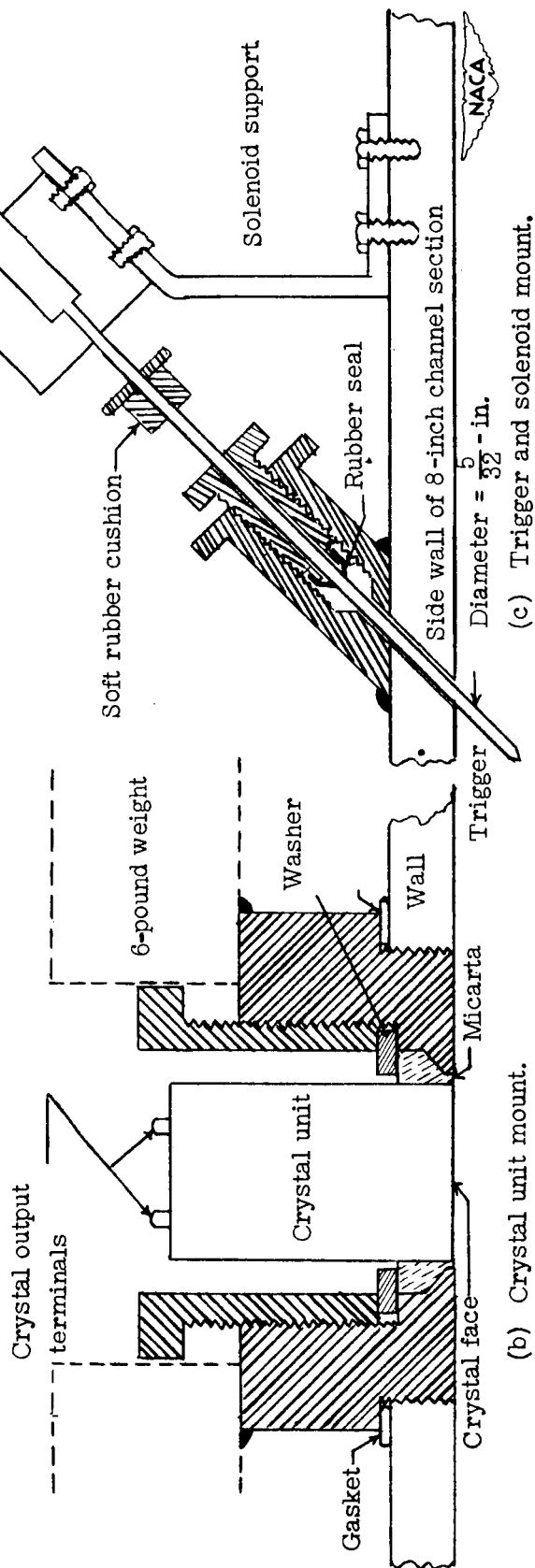


Time

Figure 6.— Pressure variation with time at reflection of expansion zone.



(a) Compression and expansion chambers.



(b) Crystal unit mount.

(c) Trigger and solenoid mount.

Figure 7.- Sketch of apparatus used to study flow.

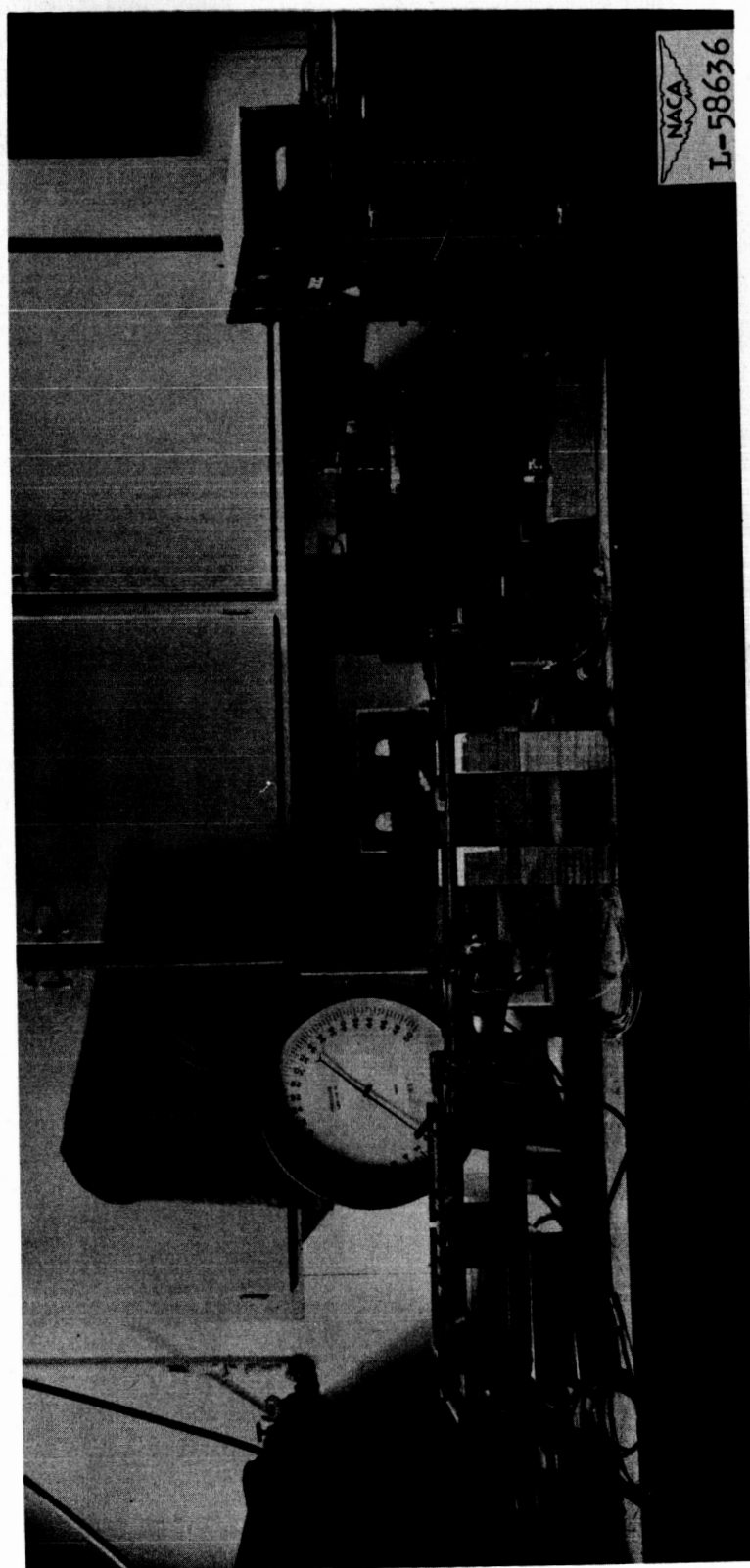


Figure 8.- Apparatus used to study flow.

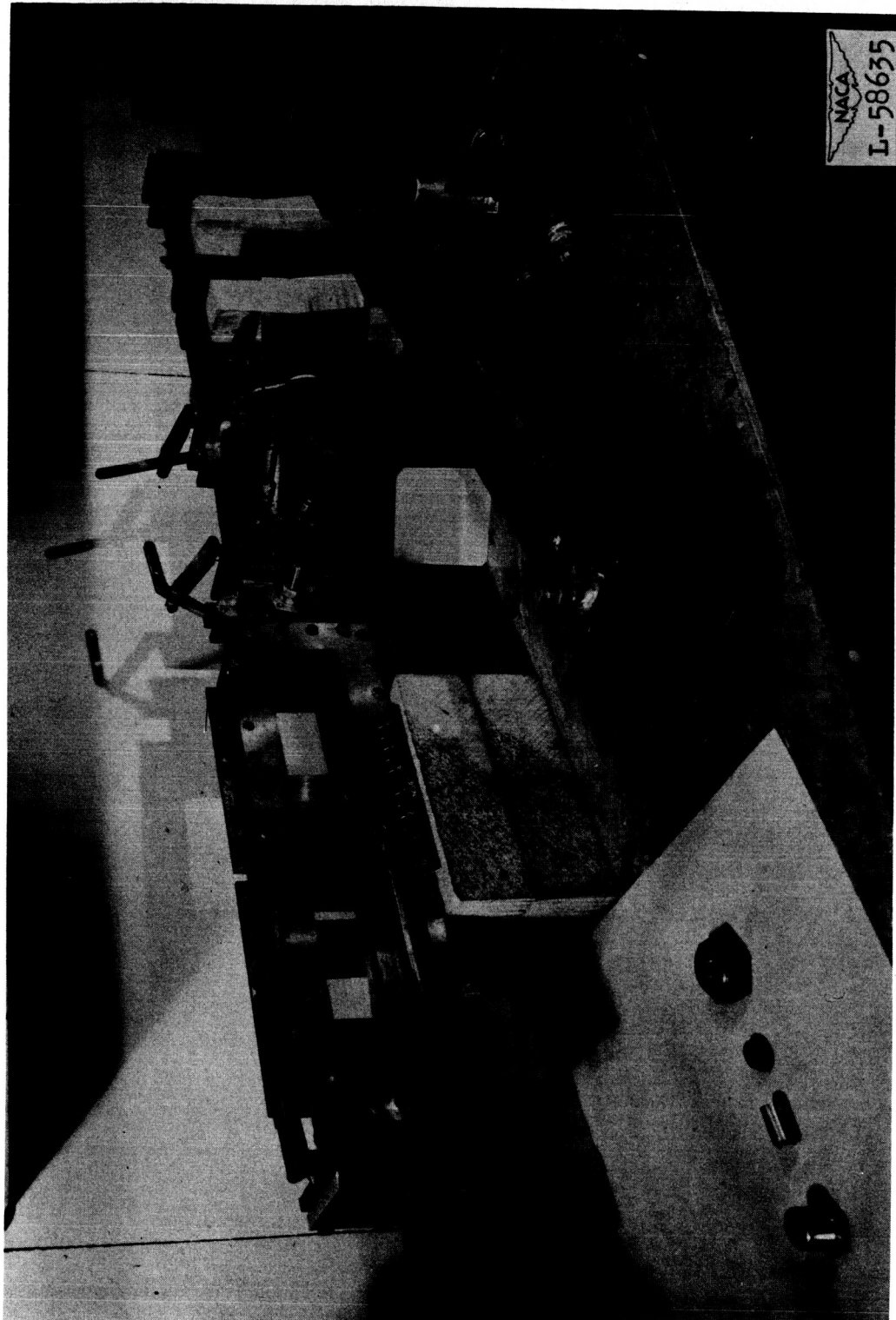


Figure 8.- Concluded.

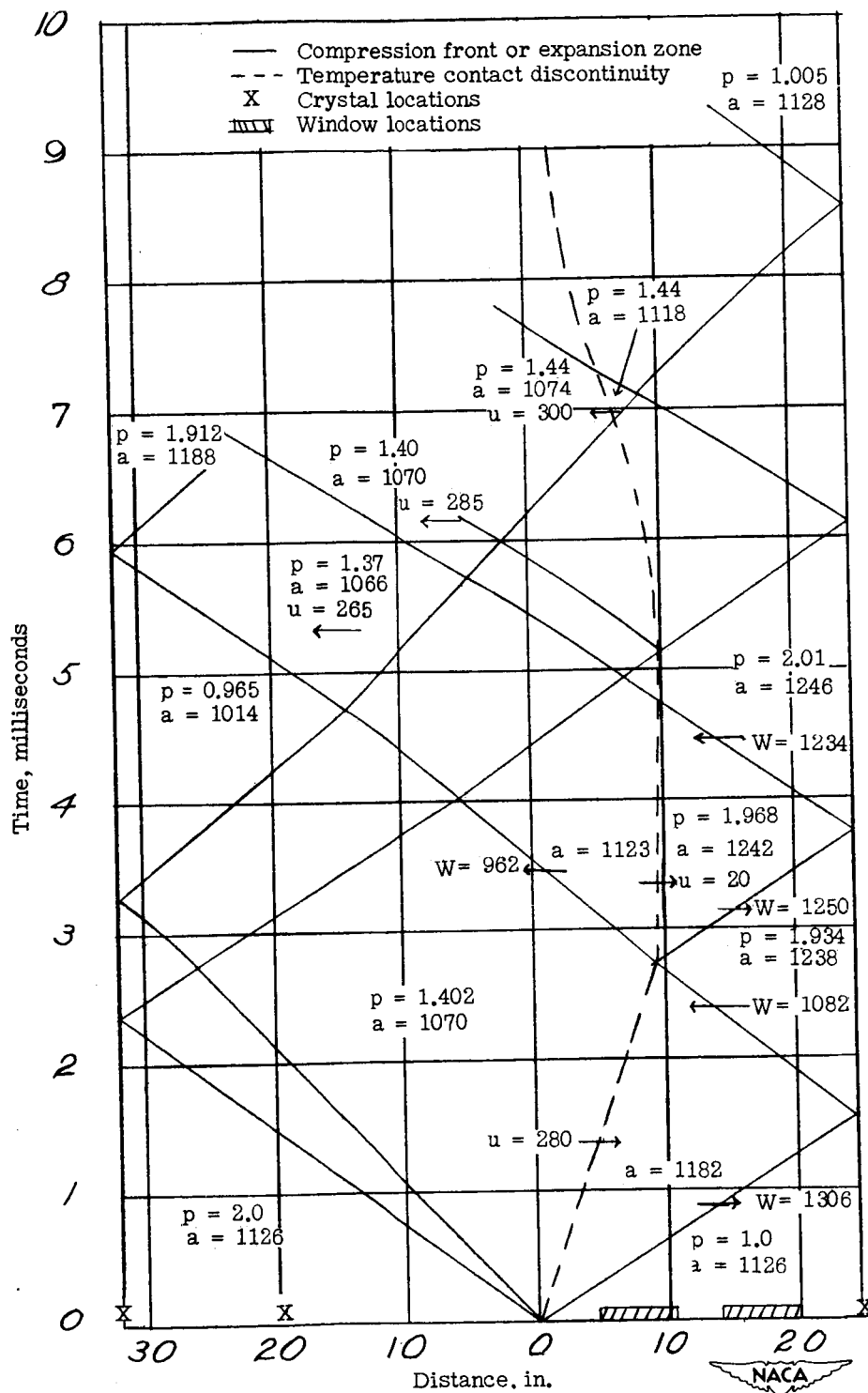
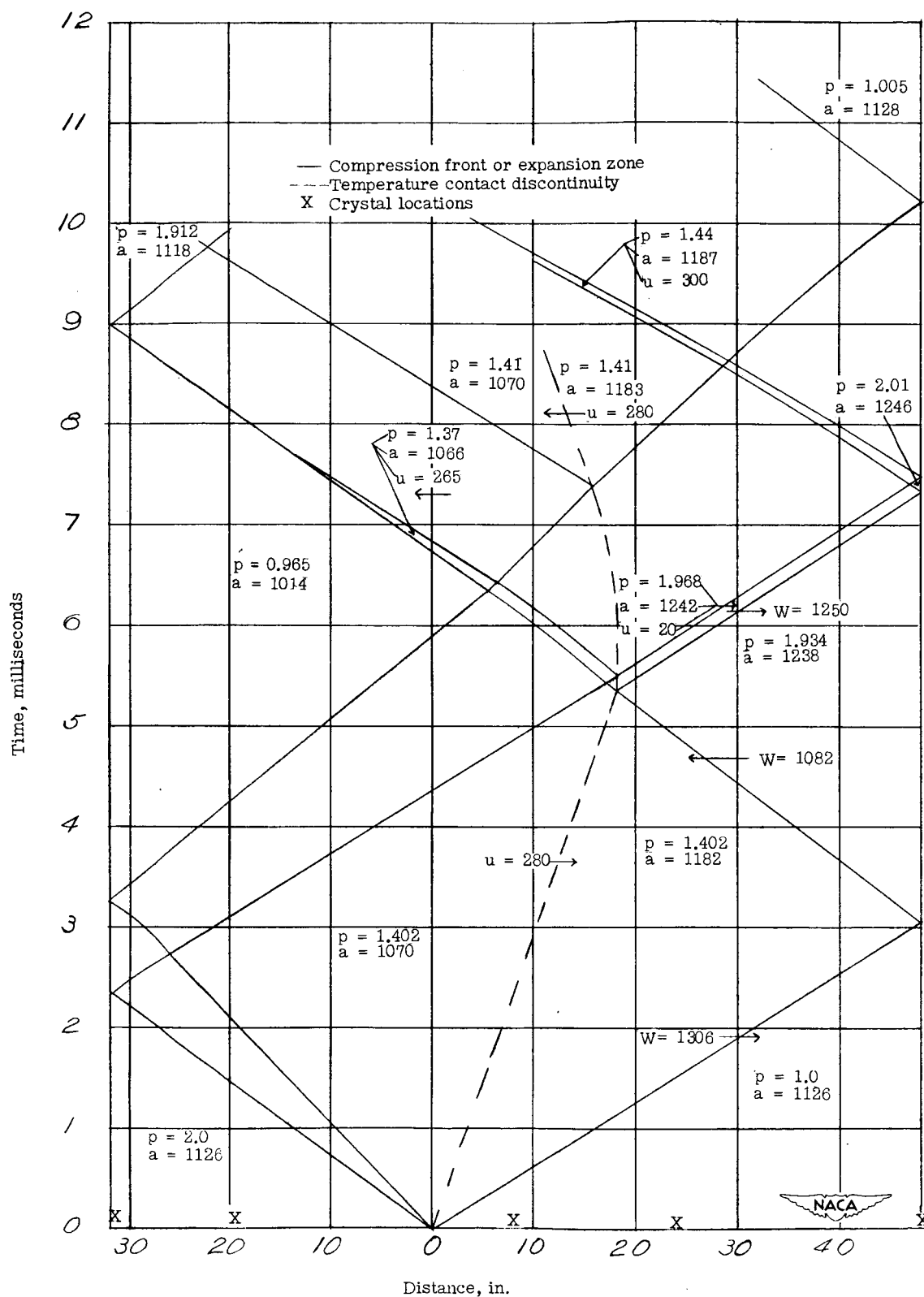
(a) $24\frac{1}{2}$ -inch low-pressure chamber.

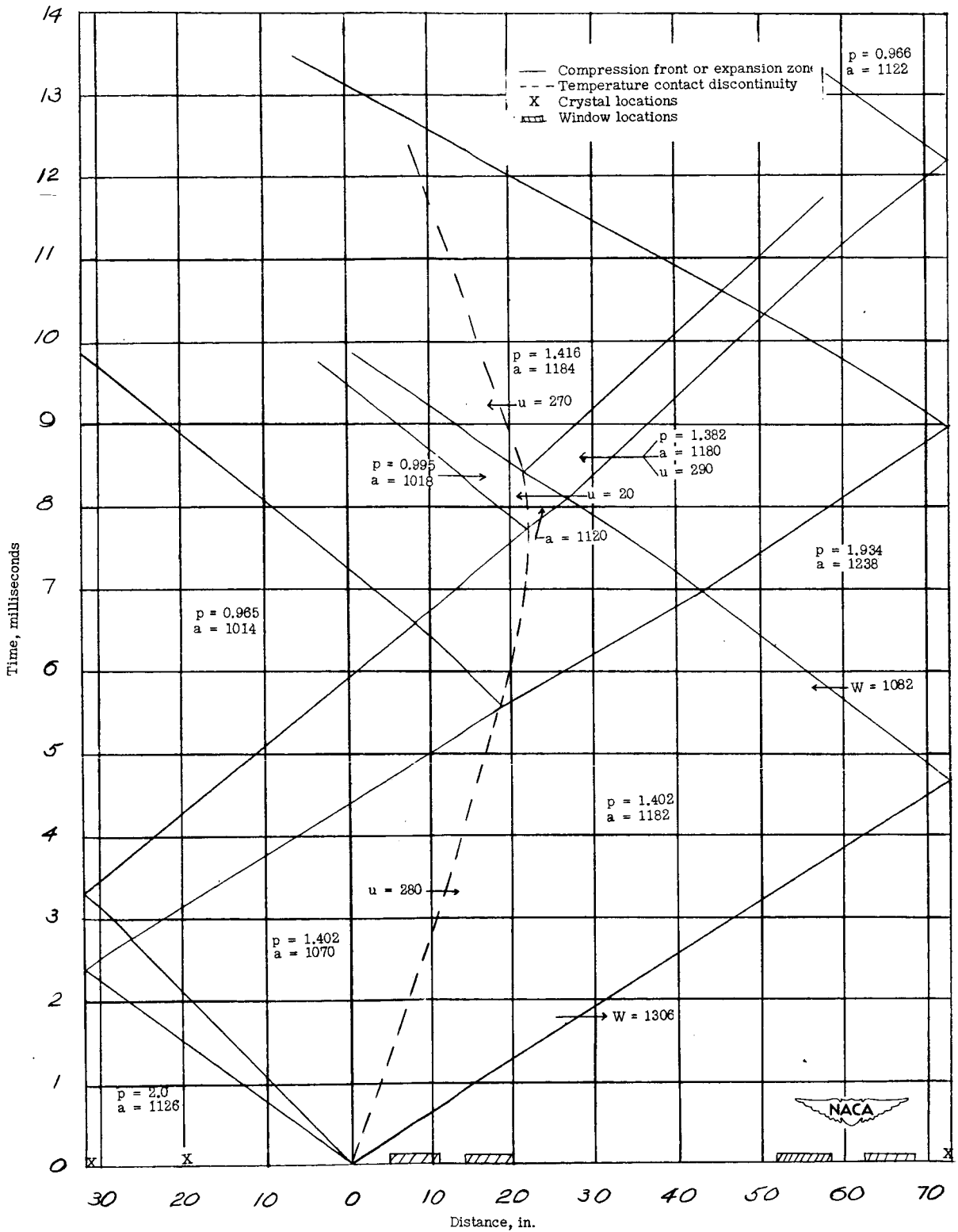
Figure 9.— Distance-time diagram for various low-pressure chambers.

$$\frac{p_0}{p_1} = 2.0; a_0 = a_1 = 1126 \text{ feet per second.}$$



(b) 48-inch low-pressure chamber.

Figure 9.— Continued.

(c) $72\frac{1}{2}$ -inch low-pressure chamber.

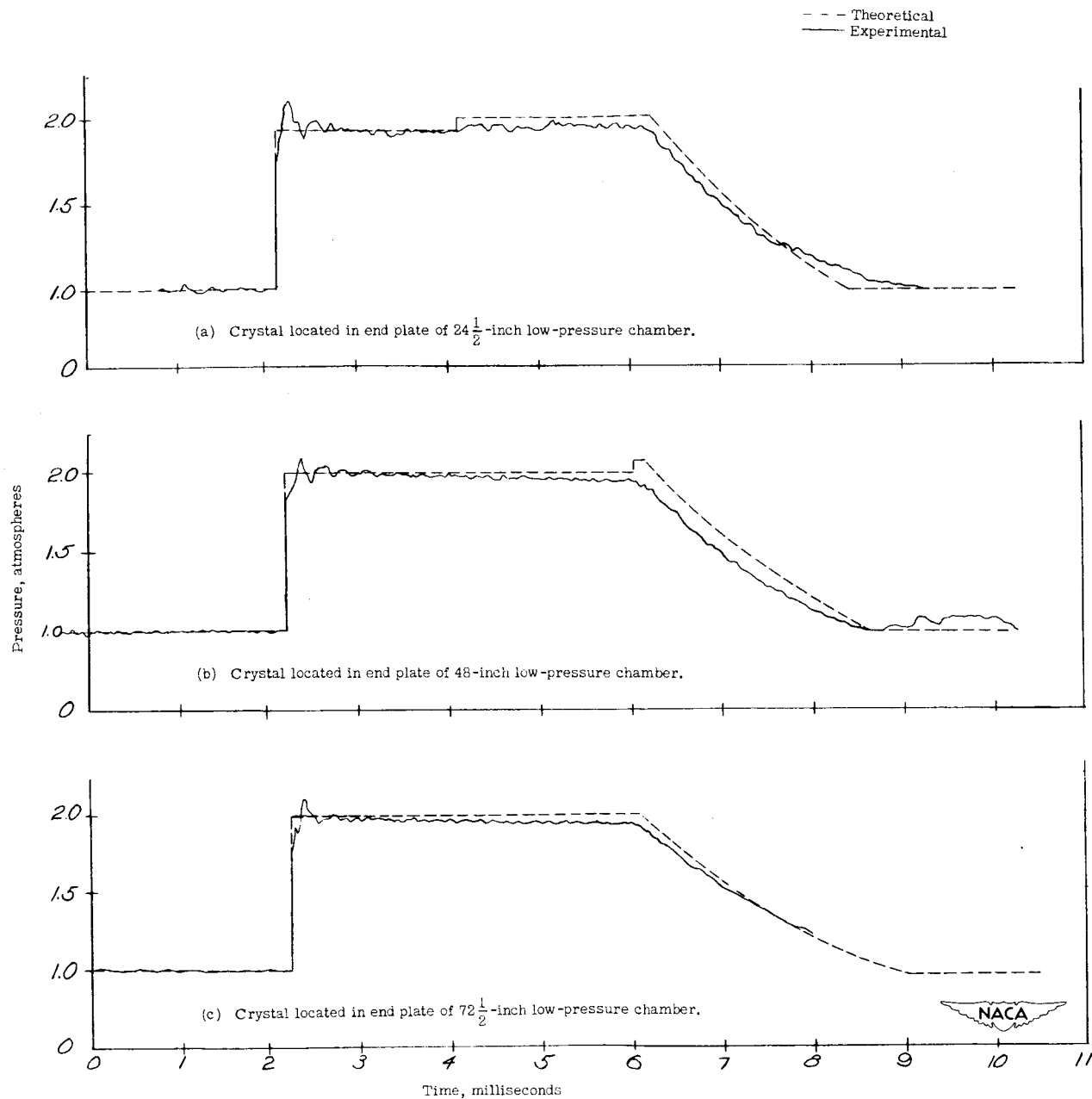


Figure 10.— Theoretical and experimental pressure-time histories for various low-pressure chambers and crystal positions plotted on same pressure-time scales. $\frac{p_0}{p_1} = 2.0$; $a_0 = a_1 = 1126$ feet per second.

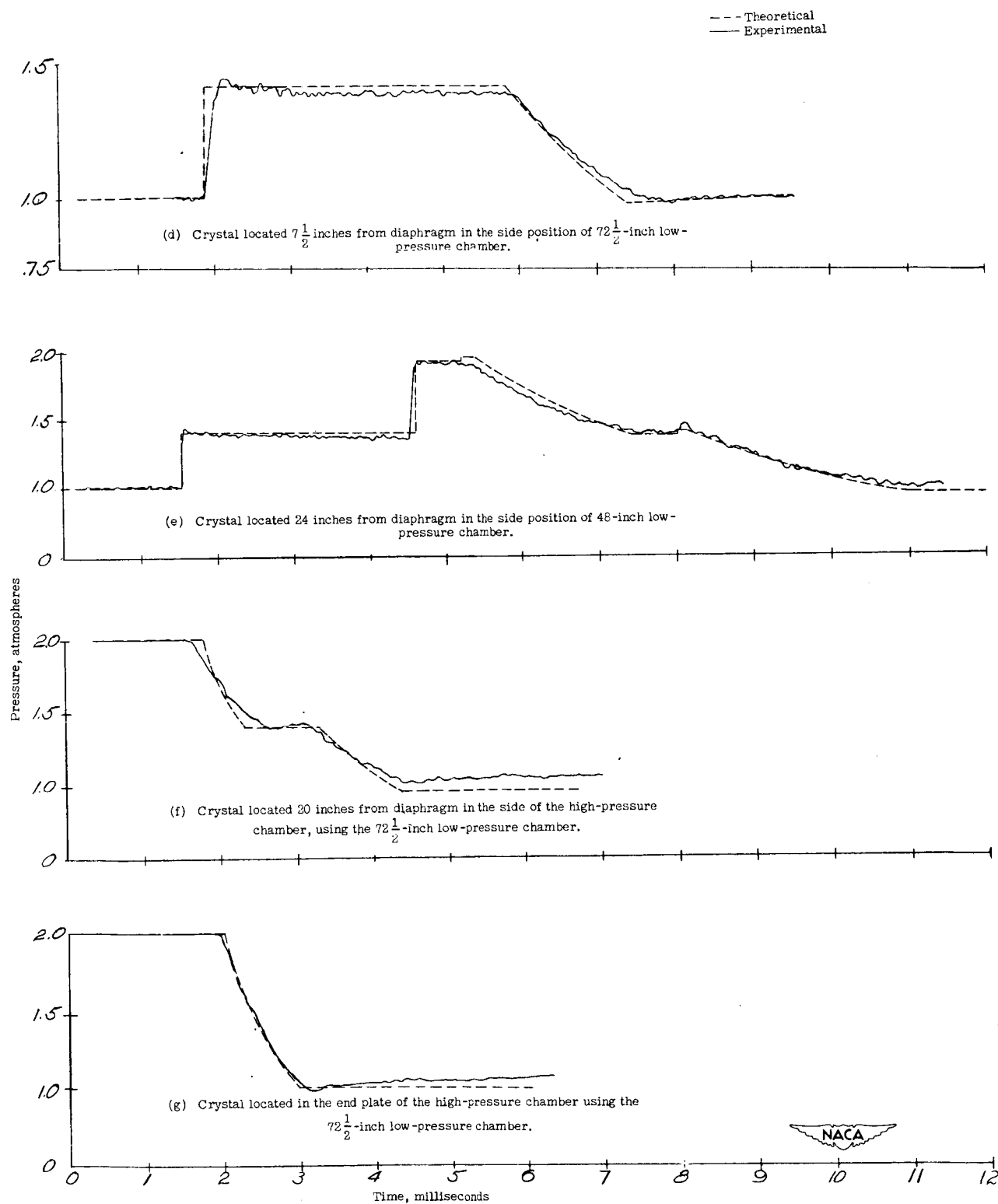
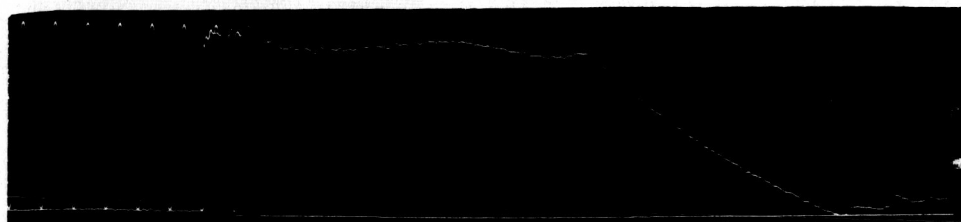


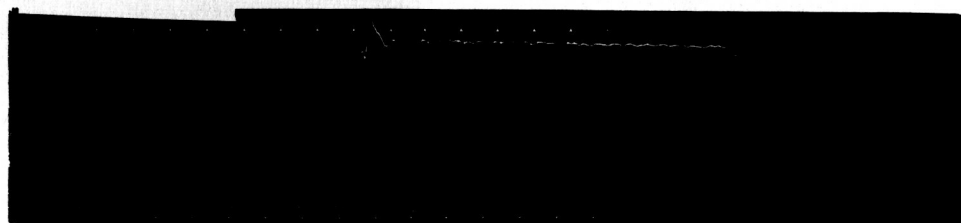
Figure 10.— Concluded.



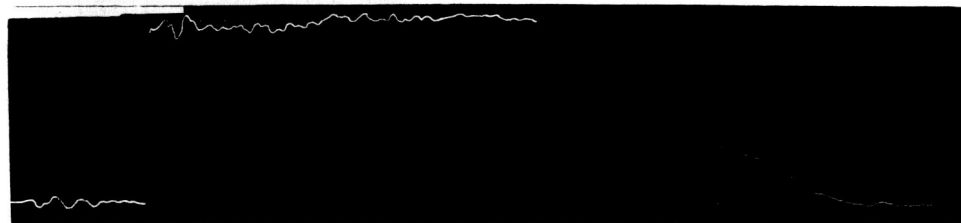
- (a) $\frac{P_0}{P_1} = 2.0$; 48-inch low-pressure chamber at end plate; end plate $\frac{3}{16}$ -inch thick plus 6-pound weight.



- (b) $\frac{P_0}{P_1} = 1.3$; $72\frac{1}{2}$ -inch low-pressure chamber at end plate.

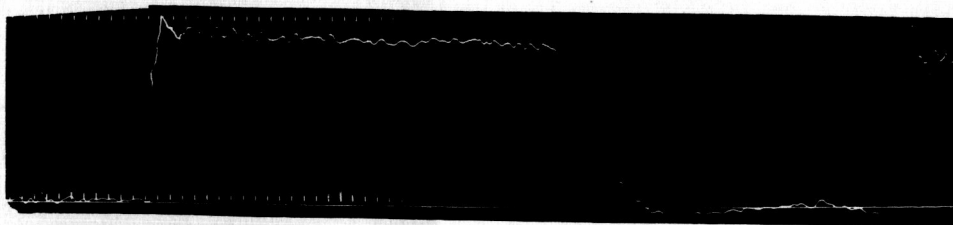


- (c) $\frac{P_0}{P_1} = 2.0$; $72\frac{1}{2}$ -inch low-pressure chamber at end plate.

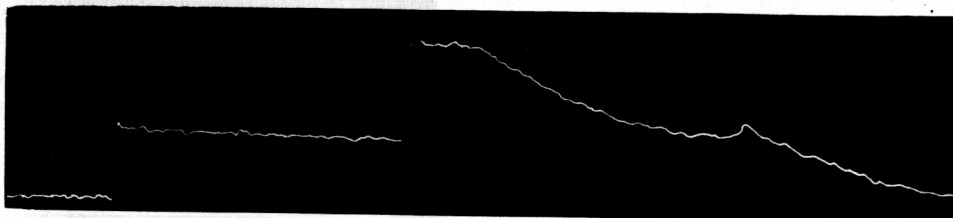


- (d) $\frac{P_0}{P_1} = 2.5$; $24\frac{1}{2}$ -inch low-pressure chamber at end plate.

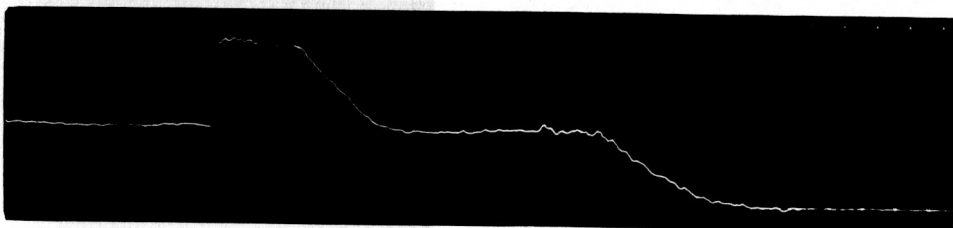
Figure 11.— Typical pressure records obtained with standard test configuration except where noted.



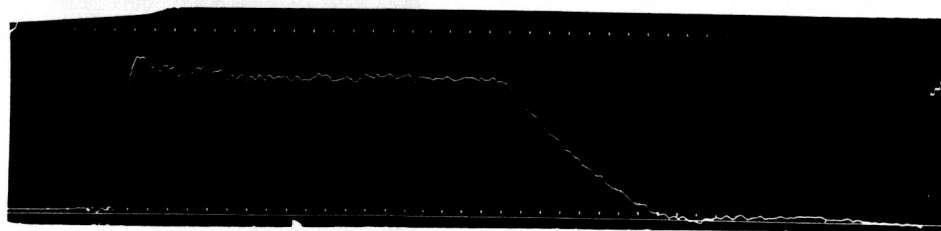
- (e) $\frac{p_0}{p_1} = 1.3$; $24\frac{1}{2}$ -inch low-pressure chamber at end plate.



- (f) $\frac{p_0}{p_1} = 2.0$; 48-inch low-pressure chamber; crystal located in the side 24 inches from diaphragm in low-pressure chamber.

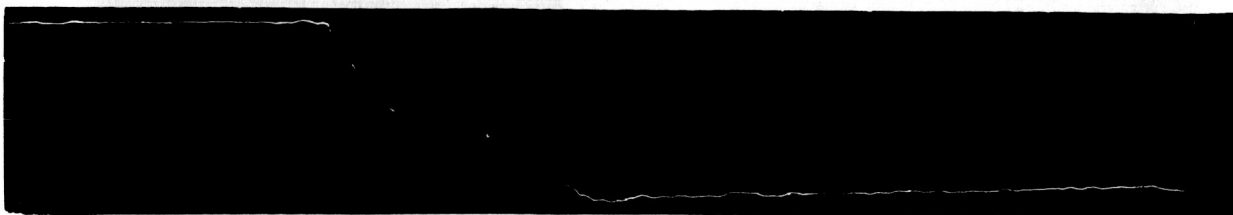


- (g) $\frac{p_0}{p_1} = 1.3$; 48-inch low-pressure chamber; crystal located in the side 24 inches from diaphragm in low-pressure chamber.

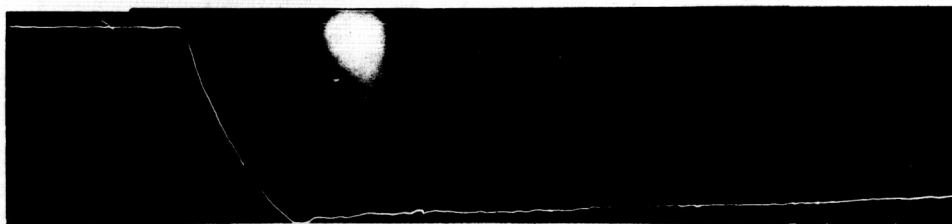


- (h) $\frac{p_0}{p_1} = 2.0$; $72\frac{1}{2}$ -inch low-pressure chamber; crystal located in the side $7\frac{1}{2}$ inches from diaphragm in low-pressure chamber.

Figure 11.- Continued.



- (i) $\frac{p_0}{p_1} = 2.0$; $72\frac{1}{2}$ -inch low-pressure chamber; crystal located in the side 20 inches from diaphragm in high-pressure chamber.



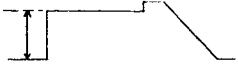
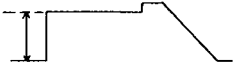




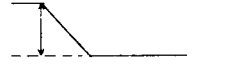
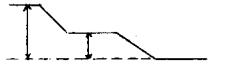

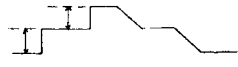
- (j) $\frac{p_0}{p_1} = 2.0$; $72\frac{1}{2}$ -inch low-pressure chamber; crystal located at end plate of high-pressure chamber.



- (k) $\frac{p_0}{p_1} = 1.3$; $72\frac{1}{2}$ -inch low-pressure chamber; crystal located at end plate of high-pressure chamber.

Figure 11.- Concluded.

TABLE II
INFORMATION REGARDING TEST CONDITIONS ON CURVES

Symbol	Crystal position	Low-pressure-chamber length (in.)	Deviation from standard test configuration	Position on test record at which voltage measurements were taken
○	End plate of low-pressure chamber	48	None	
+	-----do-----	48	End plate $\frac{3}{16}$ in. thick plus 6 lb weight	
×	-----do-----	48	$P_1 = 0.5P_a$	
◻	-----do-----	$24\frac{1}{2}$	None	
◊	-----do-----	$24\frac{1}{2}$	Without condenser	
△	-----do-----	$72\frac{1}{2}$	None	
▽	-----do-----	$72\frac{1}{2}$	None	
▷	20 in. from diaphragm in high-pressure chamber	$72\frac{1}{2}$	None	
◀	$7\frac{1}{2}$ in. from diaphragm in low-pressure chamber	$72\frac{1}{2}$	None	
◁	$24\frac{1}{2}$ in. from diaphragm in low-pressure chamber	48	None	

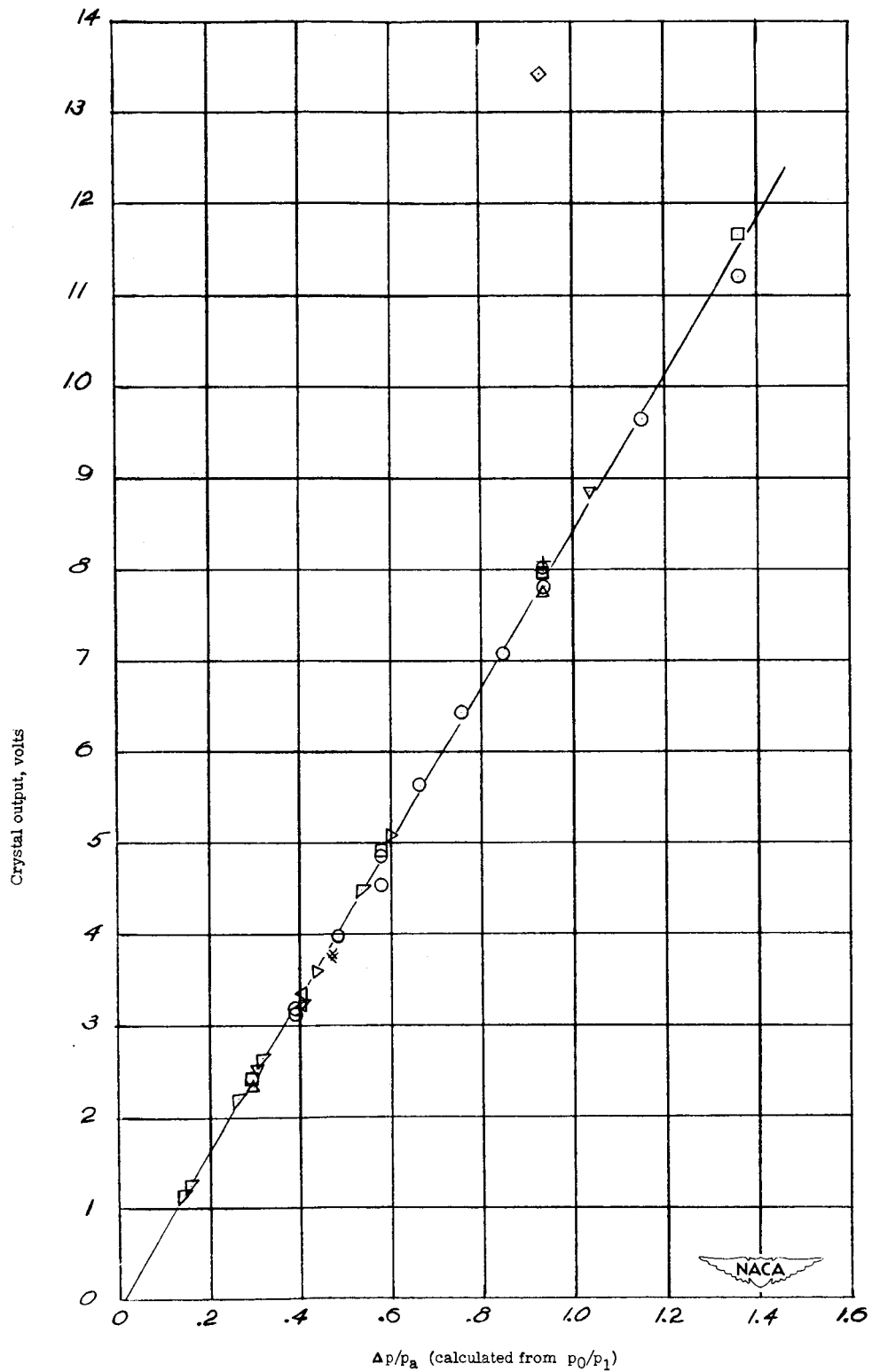


Figure 12.— Voltage output of crystal unit as a function of pressure difference experienced at crystal as a result of passing disturbance. Δp calculated from theory. (Symbols designating test conditions are identified in table II.)

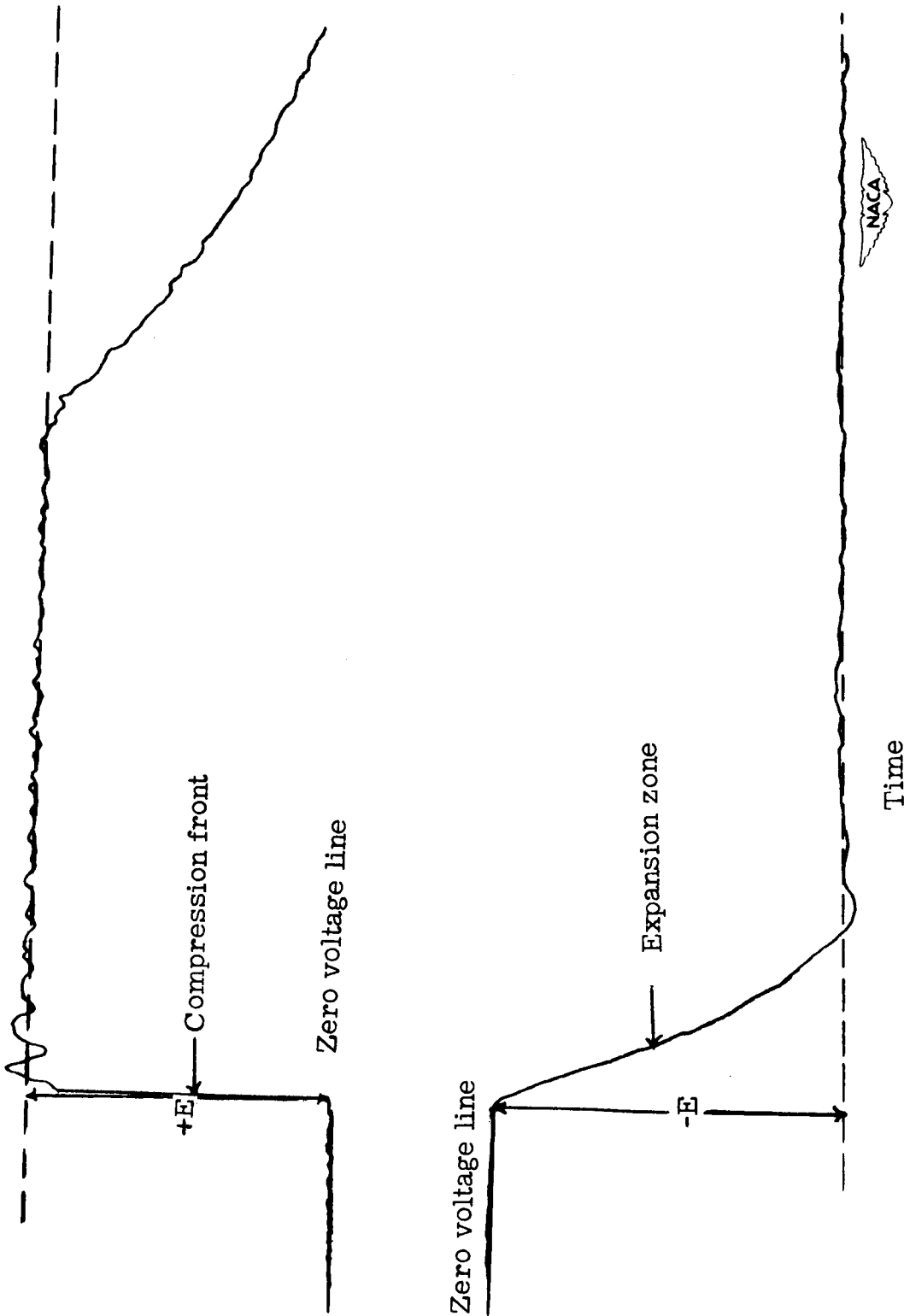
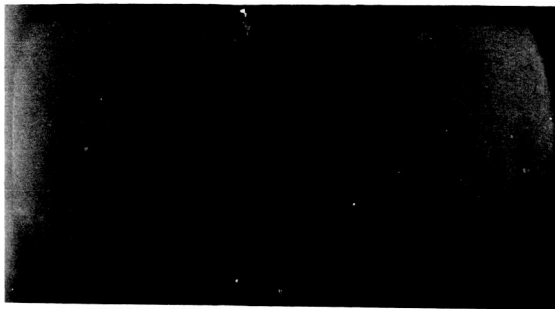
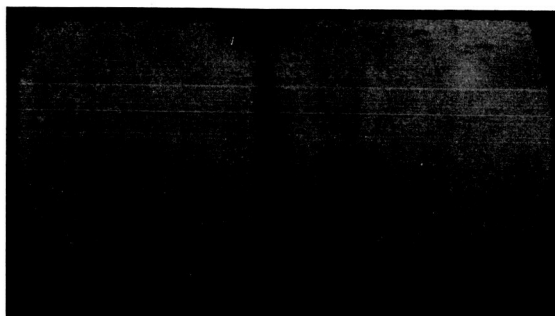


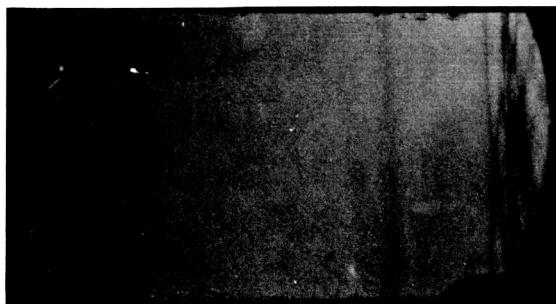
Figure 13.— Method used to measure voltage on pressure-time records.



- (a) $\frac{p_0}{p_1} = 1.6$; $24\frac{1}{2}$ -inch low-pressure chamber;
first window from diaphragm; time,
0.5 millisecond.

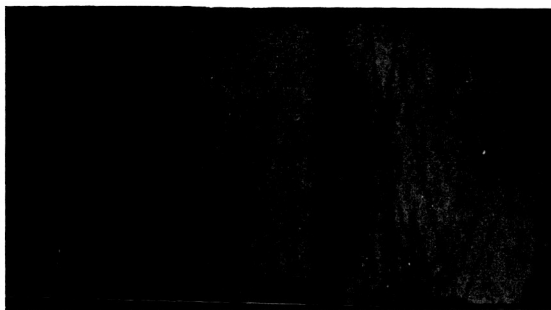


- (b) $\frac{p_0}{p_1} = 2.0$; $24\frac{1}{2}$ -inch low-pressure chamber;
first window from diaphragm; time,
0.5 millisecond.

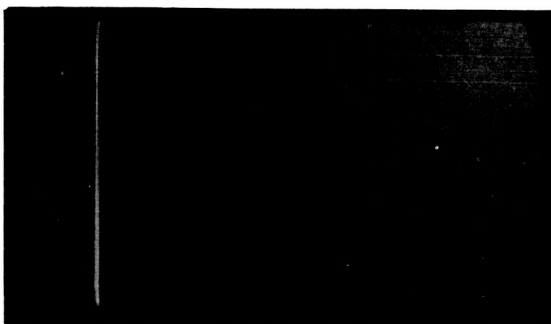


- (c) $\frac{p_0}{p_1} = 2.0$; $24\frac{1}{2}$ -inch low-pressure chamber;
second window from diaphragm; time,
0.97 millisecond.

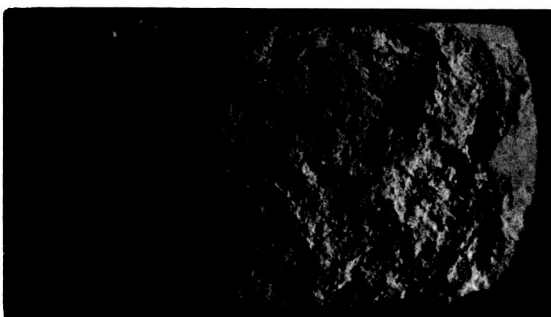
Figure 14.— Schlieren photographs taken at various times following burst of diaphragm. Positive x-direction is to the ~~right~~.
LEFT



- (d) $\frac{p_0}{p_1} = 2.0$; $24\frac{1}{2}$ -inch low-pressure chamber;
second window from diaphragm; time,
1.08 milliseconds.



- (e) $\frac{p_0}{p_1} = 2.0$; $24\frac{1}{2}$ -inch low-pressure chamber;
second window from diaphragm; time,
1.98 milliseconds; shock reflected.

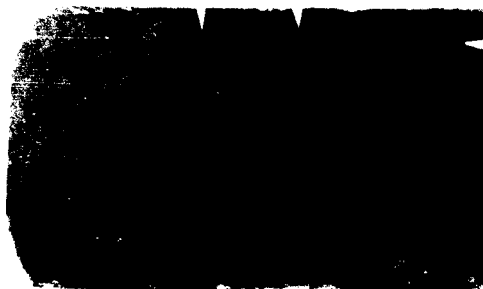


- (f) $\frac{p_0}{p_1} = 2.0$; $24\frac{1}{2}$ -inch low-pressure chamber;
first window from diaphragm; time,
2.0 milliseconds.

Figure 14.- Continued.



- (g) $\frac{p_0}{p_1} = 2.0$; $24\frac{1}{2}$ -inch low-pressure chamber;
first window from diaphragm; time,
2.7 milliseconds; shock reflected.



- (h) $\frac{p_0}{p_1} = 2.0$; $72\frac{1}{2}$ -inch low-pressure chamber;
second window from diaphragm; time,
4.22 milliseconds.



- (i) $\frac{p_0}{p_1} = 2.0$; $72\frac{1}{2}$ -inch low-pressure chamber;
second window from diaphragm; time,
5.3 milliseconds; shock reflected.

Figure 14.- Concluded.

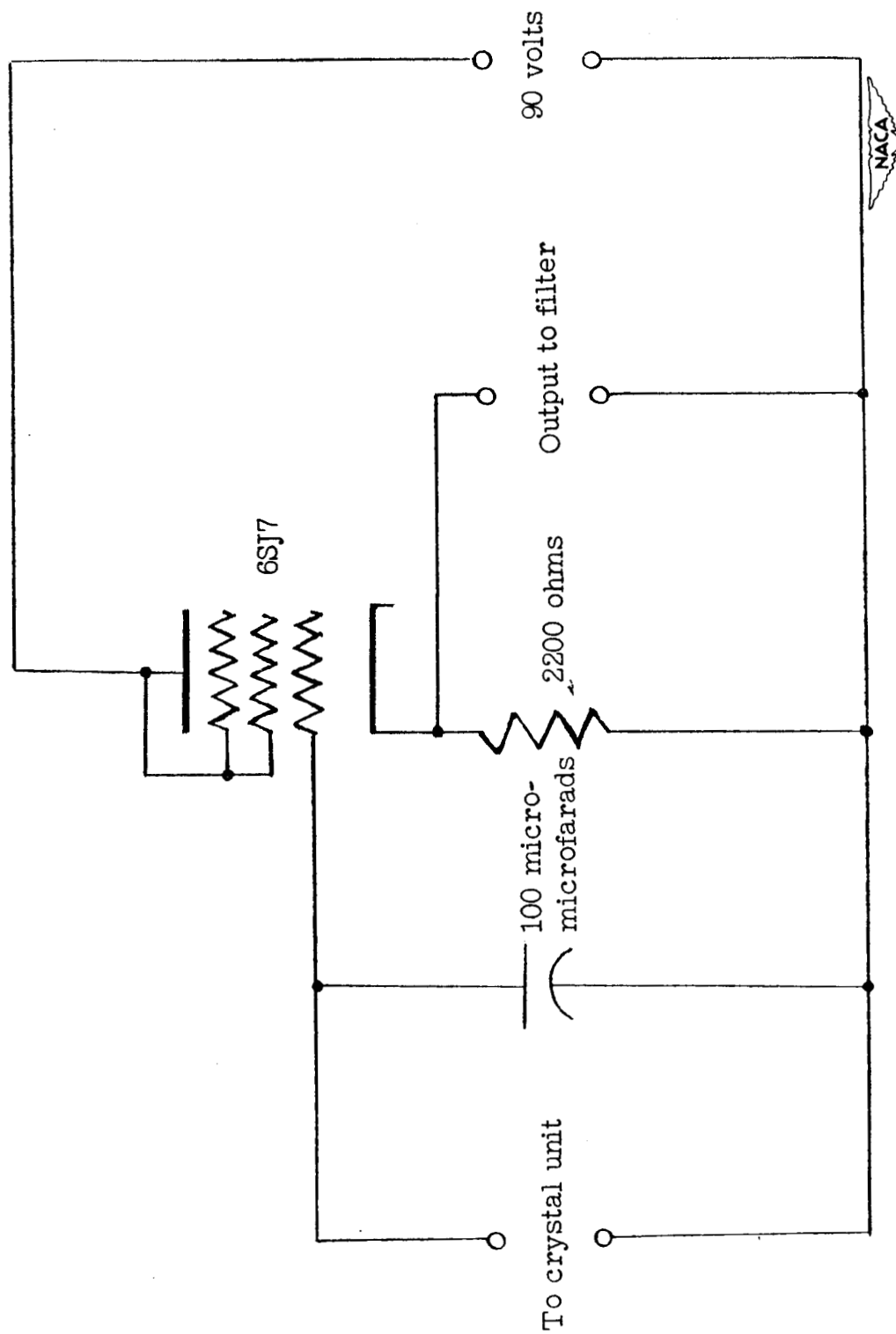


Figure 15.- Preamplifier circuit.

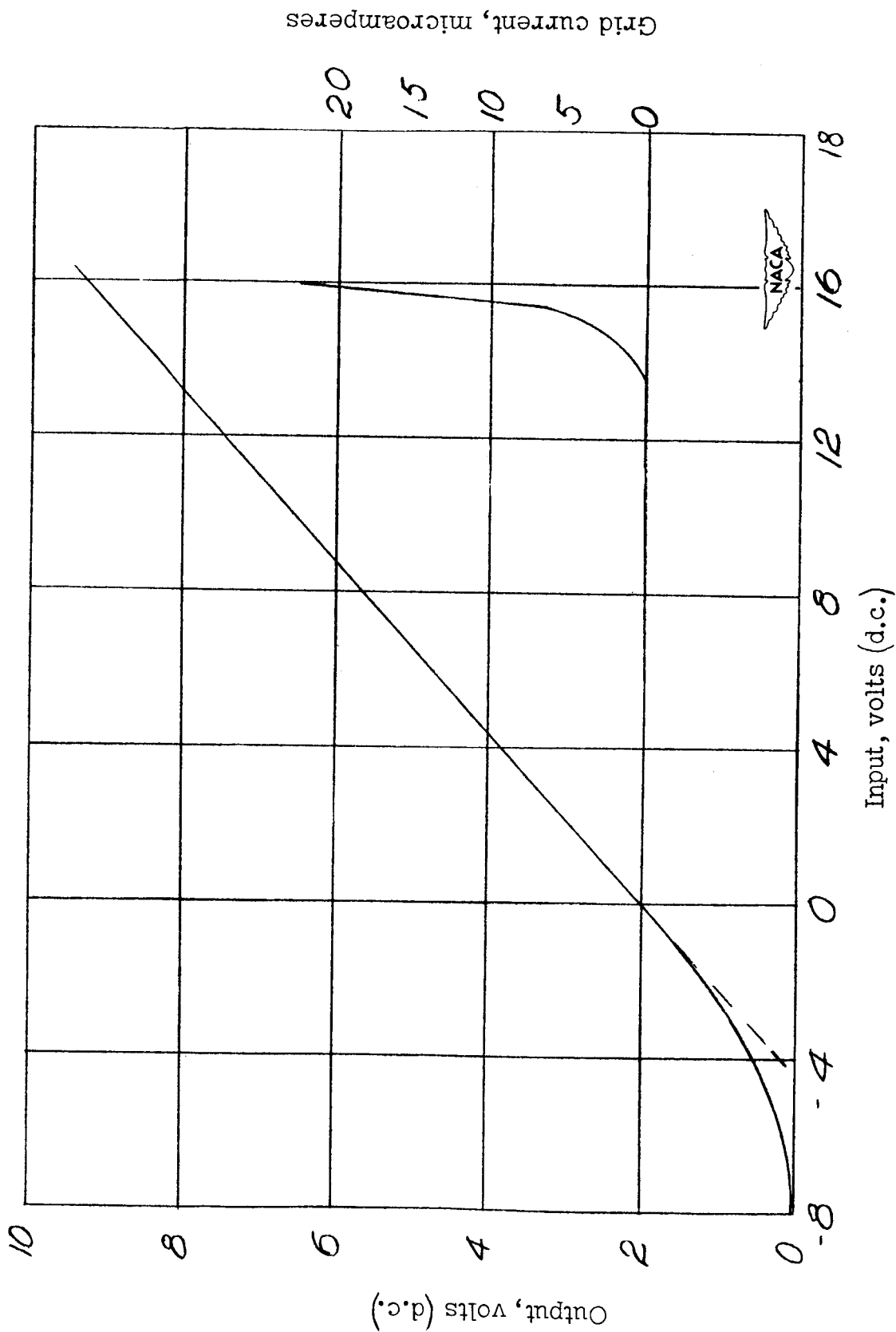
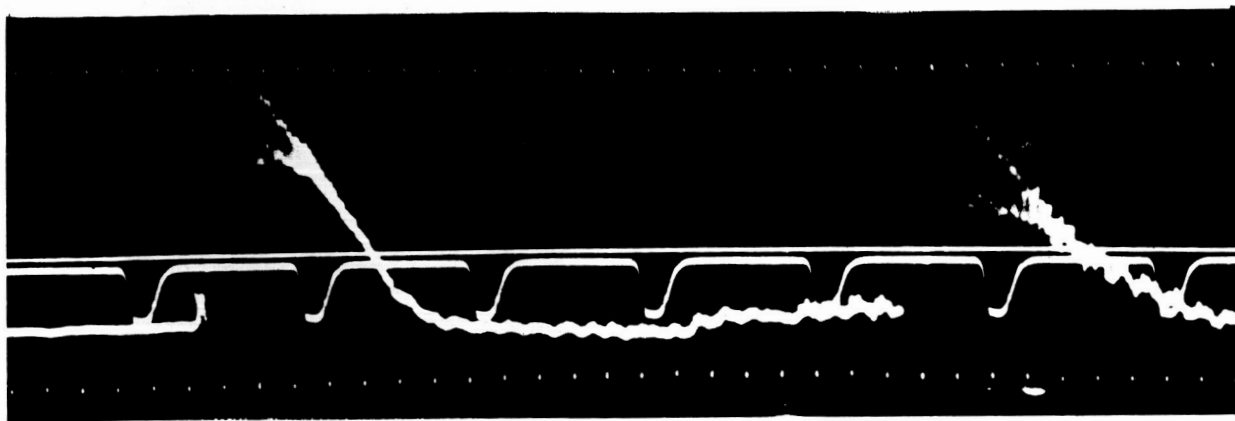
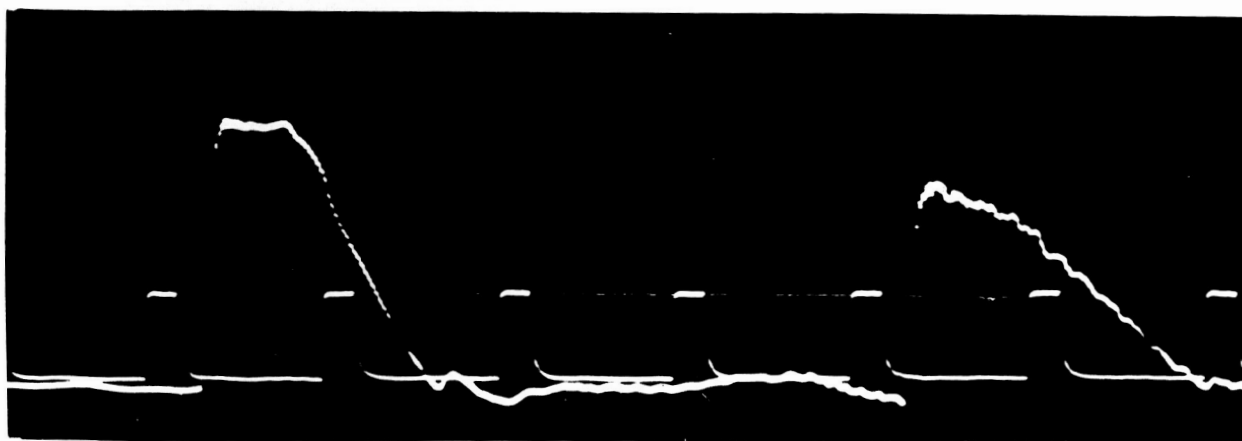


Figure 16.- Input-output voltage characteristics of the preamplifier. Plate supply voltage, 90 volts; cathode resistance, 2200 ohms.



(a) Record taken without filter in circuit.



(b) Record taken with filter in circuit.

Figure 17.- Experimental records showing attenuation of natural frequency of crystal by 47-kilocycle filter.

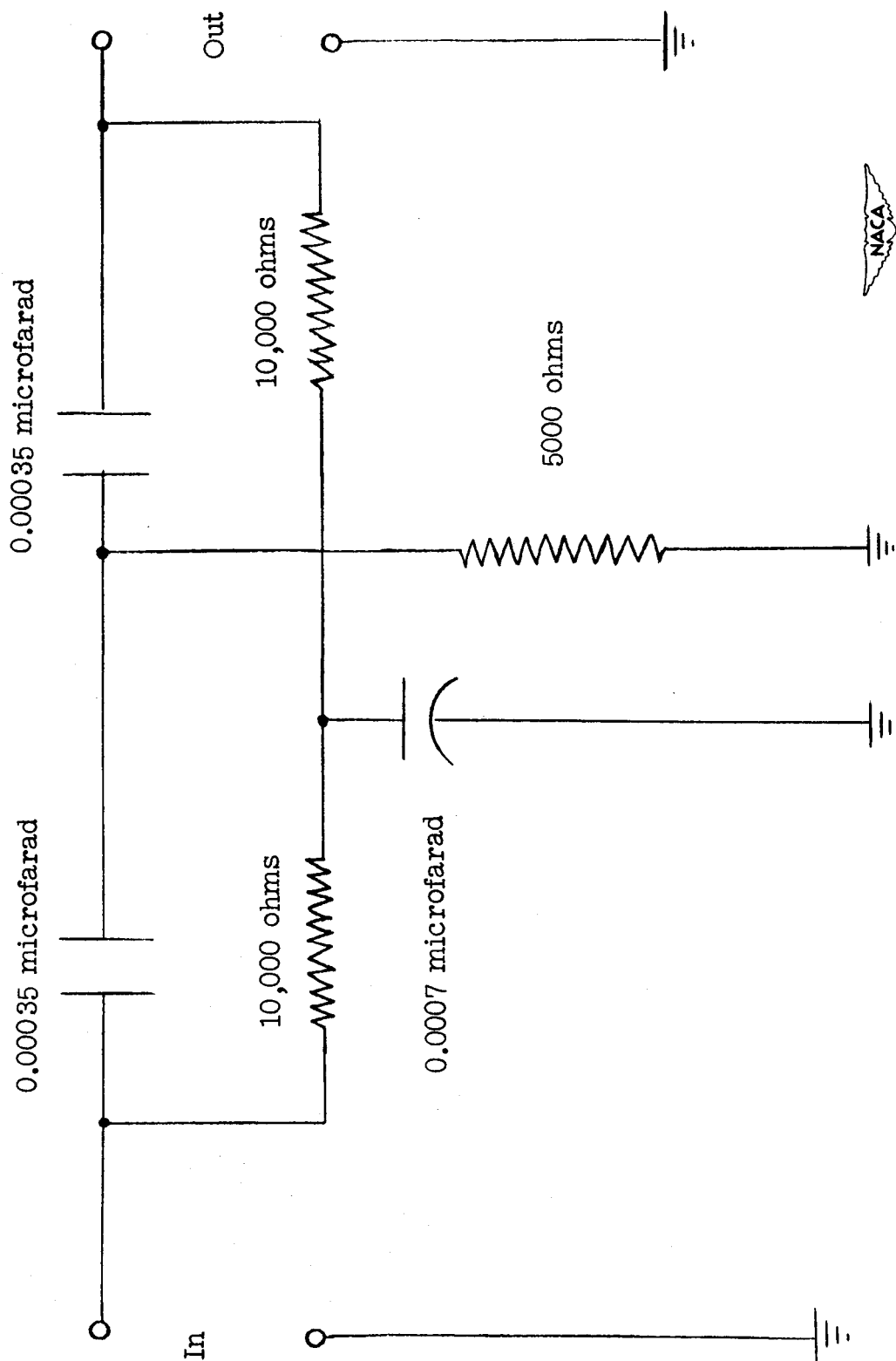
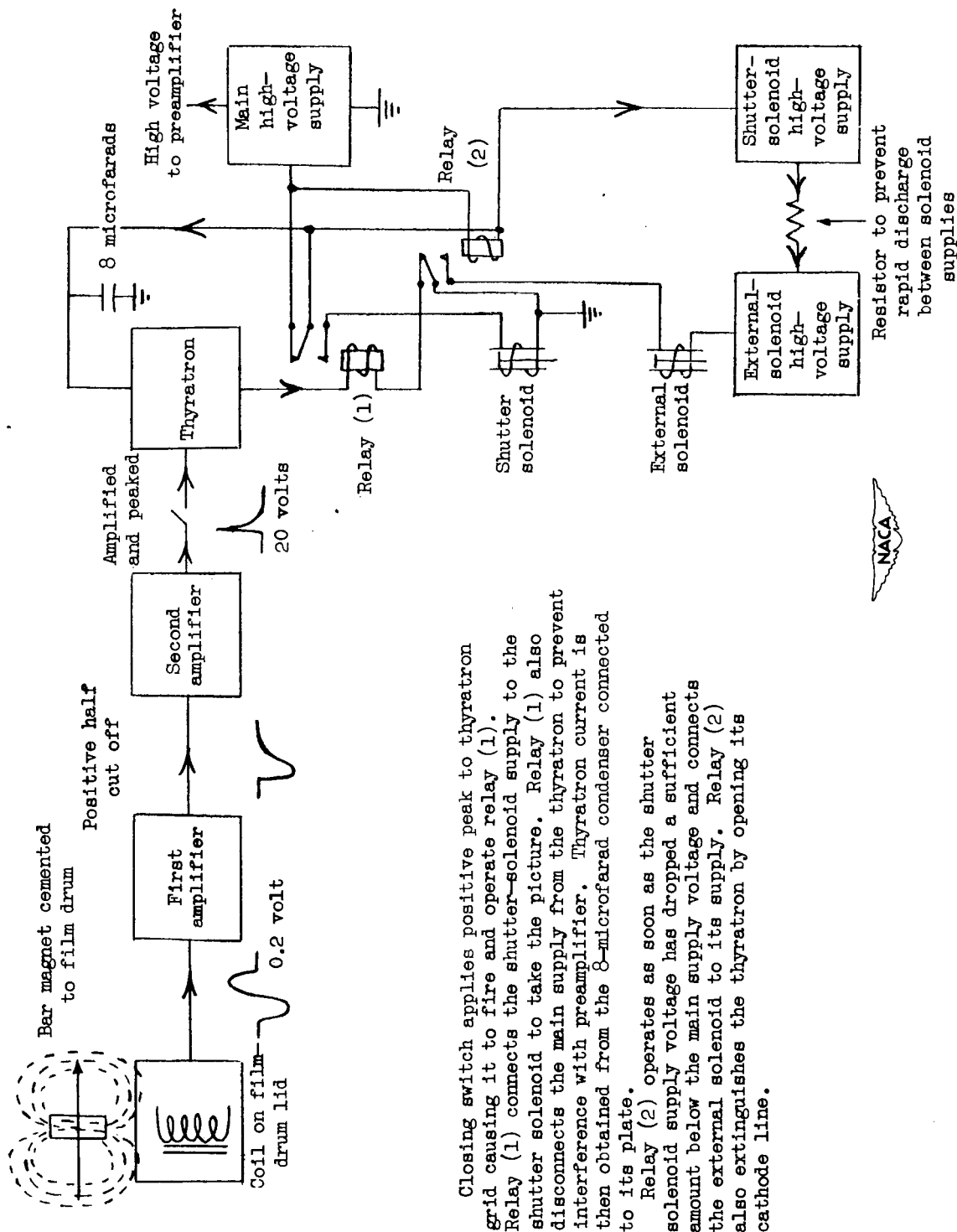


Figure 18.— Filter for removing the crystal frequency of 47 kilocycles.



Closing switch applies positive peak to thyratron grid causing it to fire and operate relay (1).

Relay (1) connects the shutter-solenoid supply to the shutter solenoid to take the picture. Relay (1) also disconnects the main supply from the thyratron to prevent interference with preamplifier. Thyratron current is then obtained from the 8-microfarad condenser connected to its plate.

Relay (2) operates as soon as the shutter solenoid supply voltage has dropped a sufficient amount below the main supply voltage and connects the external solenoid to its supply. Relay (2) also extinguishes the thyratron by opening its cathode line.

Figure 19.- High-speed camera synchronizing unit.

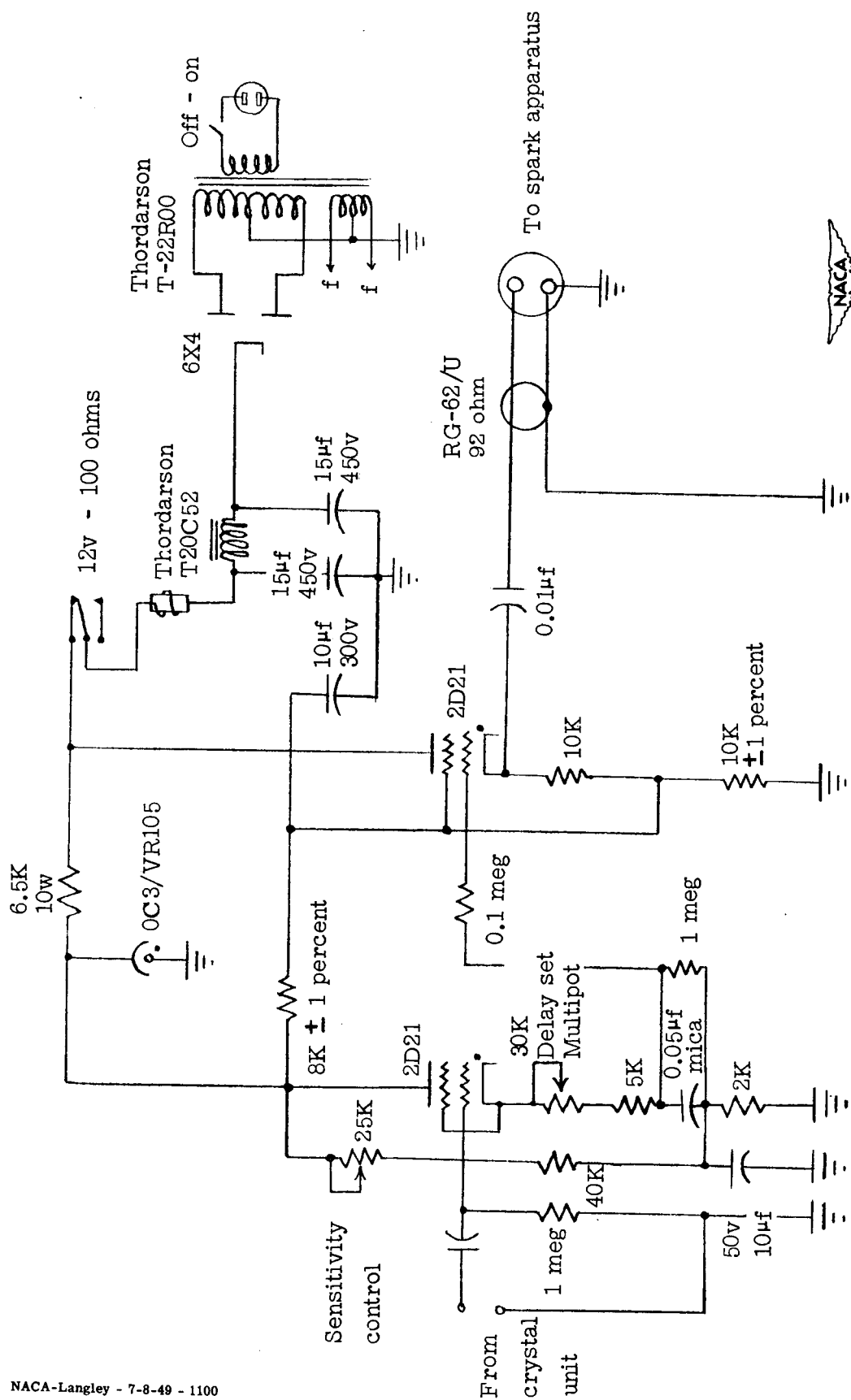


Figure 20.— Circuit for 180 to 1400 microsecond pulse delay.

(K, 1000 ohms; w, watts; meg, megohms; μ f, microfarads; v, volts.)

629.1307
-11-24

E R R A T A

NACA TN 1903

EXPERIMENTAL INVESTIGATION OF MOVING PRESSURE DISTURBANCES AND
SHOCK WAVES AND CORRELATION WITH ONE-DIMENSIONAL
UNSTEADY-FLOW THEORY

By Paul W. Huber, Cliff E. Fitton, Jr., and F. Delpino
July 1949

Figure 14: The last sentence in the title of this figure should
be changed to read "Positive x-direction is to the left".

CONN. STATE LIBRARY

NACA-Langley - 8-22-49 - 1200

AUG 29 1949